

# Measurement report: Long-term variations in surface NO<sub>x</sub> and SO<sub>2</sub> mixing ratios from 2006 to 2016 at a background site in the Yangtze River Delta region, China

Qingqing Yin<sup>1</sup>, Qianli Ma<sup>2</sup>, Weili Lin<sup>1</sup>, Xiaobin Xu<sup>3</sup>, Jie Yao<sup>2</sup>

5 <sup>1</sup> College of Life and Environmental Sciences, Minzu University of China, Beijing 100081, China

<sup>2</sup> Lin'an Atmosphere Background National Observation and Research Station, Lin'an 311307, Hangzhou, China

<sup>3</sup> Key Laboratory for Atmospheric Chemistry, Chinese Academy of Meteorological Sciences, Beijing 100081, China

*Correspondence to:* Weili Lin (linwl@muc.edu.cn)

**Abstract.** China has been experiencing rapid changes in emissions of air pollutants in recent decades. Increased emissions of primary particulates and reactive gases caused severe haze in several polluted regions including the Yangtze River Delta (YRD). Measures implemented in recent years for improving air quality have reduced the emissions of NO<sub>x</sub>, SO<sub>2</sub>, etc. The emission changes of these gases are reflected by tropospheric columns from satellite observations and surface measurements of surface concentrations from urban sites. However, little is known about the long-term variations in regional background NO<sub>x</sub> and SO<sub>2</sub>. In this study, we present NO<sub>x</sub> and SO<sub>2</sub> measurements from the Lin'an station (LAN, 119°44' E, 30°18' N, 138.6 m a.s.l.), one of the Global Atmosphere Watch (GAW) stations in China. We characterize the seasonal and diurnal variations and study the long-term trends of NO<sub>x</sub> and SO<sub>2</sub> mixing ratios observed at LAN from 2006 to 2016. We also interpret the observed variations and trends in term of changes in meteorological conditions as well as emission of these gases. The overall average mixing ratios of NO<sub>x</sub> (NO<sub>2</sub>) and SO<sub>2</sub> during 2006–2016 were  $13.6 \pm 1.2$  ppb ( $12.5 \pm 4.6$ ) and  $7.0 \pm 4.2$  ppb, respectively. The averaged seasonal variations showed maximum values of NO<sub>x</sub> and SO<sub>2</sub> in December ( $23.5 \pm 4.4$  ppb) and January ( $11.9 \pm 6.2$  ppb), respectively, and minimum values of  $7.1 \pm 0.8$  ppb and  $2.8 \pm 2.3$  ppb (both in July), respectively. The average diurnal variation characteristics of NO<sub>x</sub> and SO<sub>2</sub> differed considerably from each other though the daily average mixing ratios of both gases were significantly correlated ( $R^2 = 0.29$ ,  $P < 0.001$ ). The annual average mixing ratio of NO<sub>x</sub> increased during 2006–2011 and then decreased significantly at  $0.78$  ppb/yr ( $-5.16$  %/yr,  $P < 0.01$ ). The annual 95 % and 5 % percentiles of hourly NO<sub>x</sub> mixing ratios showed upward trends until 2012 and 2014, respectively, before a clear decline. The annual average mixing ratio of SO<sub>2</sub> decreased significantly at  $0.99$  ppb/yr ( $-8.27$  %/yr,  $P < 0.01$ ) from 2006–2016. The annual 95 % and 5 % percentiles of hourly SO<sub>2</sub> mixing ratios all exhibited significant ( $P < 0.001$ ) downward trends at  $3.18$  ppb/yr and  $0.19$  ppb/yr, respectively. Changes in the total NO<sub>x</sub> and SO<sub>2</sub> emissions as well as the industrial emissions in the YRD region were significantly correlated with the changes in annual NO<sub>x</sub> and SO<sub>2</sub> mixing ratios. The significant decreases in NO<sub>x</sub> from 2011 to 2016 and SO<sub>2</sub> from 2006 to 2016 highlight the effectiveness of relevant control measures on the reduction in NO<sub>x</sub> and SO<sub>2</sub> emissions in the YRD region. A decrease of annual SO<sub>2</sub>/NO<sub>x</sub> ratio was found, suggesting a better efficacy in the emission reduction of SO<sub>2</sub> than NO<sub>x</sub>. We found gradual changes in average diurnal patterns of NO<sub>x</sub> and SO<sub>2</sub>, which could be attributed to increasing contributions of vehicle emissions to NO<sub>x</sub> and weakening impacts of large sources on the SO<sub>2</sub> concentration.

This study reaffirms China's success in controlling both NO<sub>x</sub> and SO<sub>2</sub> in the YRD but indicate at the same time a necessity to strengthen the NO<sub>x</sub> emission control.

35 **Keywords:** background NO<sub>x</sub> and SO<sub>2</sub>; long-term trend; emission reduction.

## 1 Introduction

China's economy has experienced decades of rapid development, resulting in considerable pollutant emissions from coal combustion and motor vehicles, which affect ambient air quality and human health (Kan et al., 2009, 2012; Liang et al., 2019). NO<sub>x</sub> and SO<sub>2</sub> are two major gaseous pollutants that are essential precursors to secondary aerosol formation and acidification  
40 (Li et al., 2020). Therefore, the changes in NO<sub>x</sub> and SO<sub>2</sub> emissions have been receiving increasing attention in China (Zhao et al., 2013; Zhao et al., 2018). To improve air quality, the Chinese government has promulgated a series of policies and regulations on SO<sub>2</sub> and NO<sub>x</sub> control, especially since 2006 and 2011, respectively (Zheng et al., 2015).

Long-term observations of NO<sub>x</sub> and SO<sub>2</sub> are not only critical for the integrated assessment of air quality and atmosphere–  
biosphere interactions (Swartz et al., 2020a), but also for the analysis of their reduction effects on PM<sub>2.5</sub>, nitrate, sulphate, and  
45 near-surface O<sub>3</sub>, providing a basis for further improvement of atmospheric protection policies (Yu et al., 2019). At a regional scale, long-term, reliable NO<sub>x</sub> and SO<sub>2</sub> observations can also provide data to enable the scientific community to predict the future state of the atmosphere and assess environmental policies, serving to reduce environmental risks and enhance climate, weather, and air quality prediction capabilities (GAW, 2017). Numerous studies have evaluated the effectiveness of NO<sub>x</sub> and SO<sub>2</sub> control in China from a long-term perspective by using emission inventories, satellite retrieval data, and ground monitoring  
50 data. For example, Sun et al. (2018) used a unified source emission inventory approach to quantify the historical emission trends of SO<sub>2</sub> and NO<sub>x</sub> in China from 1949 to 2015; the results indicated that these pollutants reached an inflection point in 2006 and 2011, respectively. Source emission inventories by Kurokawa and Ohara (2020) revealed similar patterns. During the period from January 2005 to December 2015, the column concentration of NO<sub>2</sub> from ozone monitoring instrument (OMI) satellite retrieval indicated an increasing trend in most of China until a gradual or slight decrease in 2011 or 2012 (Cui et al.,  
55 2016). Zhao et al. (2019) used ground-based NO<sub>2</sub> observations to assess the effectiveness of pollution control policy in a southwestern city cluster and revealed fluctuations in NO<sub>2</sub> mixing ratios from 2008 to 2013, followed by an irregular declining trend after 2013. All these studies reported that NO<sub>x</sub> and SO<sub>2</sub> mixing ratios have been effectively controlled in China despite the increasing economic development over the past decades.

The Yangtze River Delta (YRD) region is located in the central-eastern region of China, which has the largest economic output  
60 in China and has the sixth largest urban agglomeration in the world. The region covers an area of 359,100 km<sup>2</sup> and has a population of 224 million, accounting for 16.08 % of the country's population (Fang and Tian, 2020). Because of increases in population, urbanization, and industrialization in recent decades, the air pollution in the YRD has exhibited complex and regional characteristics (Li et al., 2019; Wang et al., 2019), and the YRD has become one of the most polluted regions in the world (Xie, 2017b), with NO<sub>x</sub> and SO<sub>2</sub> being the main factors that influence air quality in the region (Yang and Luo, 2019).

65 Xu et al. (2008) compared observational data in 2005–2006 with those 10 years earlier and concluded that as early as the mid-  
1990s, SO<sub>2</sub> and NO<sub>x</sub> mixing ratios had already become considerably high at the background station in the YRD; since then,  
anthropogenic emissions have caused a substantial increase in the NO<sub>x</sub> concentration, making NO<sub>x</sub> another major pollutant in  
addition to SO<sub>2</sub>. The implementation of pollution control policies and continual innovation in SO<sub>2</sub> pollution control technology  
have mitigated SO<sub>2</sub> pollution in the YRD, resulting in a consistent decrease in SO<sub>2</sub> mixing ratios (Qi et al., 2012); however,  
70 NO<sub>x</sub> mixing ratios remain high (Shi et al., 2018).

In this paper, we present 11-year (2006–2016) surface NO<sub>x</sub> and SO<sub>2</sub> observation data from Lin'an regional atmospheric  
background station. We analysed the long-term variations of NO<sub>x</sub> and SO<sub>2</sub> and their influencing factors in the YRD background  
area to (1) assess the effectiveness of pollution control in the area and (2) provide a scientific basis and reference for future  
pollution control strategies.

## 75 **2 Information and methods**

### **2.1 Site information**

The Lin'an regional atmospheric background monitoring station (119°44' E, 30°18' N, 138.6 m a.s.l.; referred to LAN) is  
located in Lin'an District, Hangzhou City, Zhejiang Province (Fig. 1) and is one of the regional atmospheric background  
stations operated by China Meteorological Administration; it is also a World Meteorological Organization (WMO) Global  
80 Atmospheric Watch (GAW) member station. LAN is located on an isolated hilltop, surrounded by hilly and mountainous  
terrain, with no large villages within a 3 km radius. It is within the region of subtropical monsoon climate, with the most  
dominant wind direction from the northeast and the secondary from the southwest. The seasonal variations in meteorological  
elements, namely atmospheric pressure (P), temperature (T), wind speed (WS), relative humidity (RH), and rose maps of wind  
speed (WS) and wind direction frequency (WF), are presented in Fig. 2.

### 85 **2.2 Observations and quality control methods**

At the LAN station, observations of O<sub>3</sub>, NO<sub>x</sub>, SO<sub>2</sub>, and CO are performed by an integrated observation and quality control  
system combining O<sub>3</sub>, NO<sub>x</sub>, SO<sub>2</sub>, and CO analysers, calibration equipment, and ancillary materials, such as standard gases and  
zero air supply (Lin et al., 2009). NO<sub>x</sub> and SO<sub>2</sub> were measured using a Model 42C-TL trace-level chemiluminescent analyser  
and a Model 43C-TL trace-level pulsed fluorescence analyser (Thermo Fishier Scientific, MA, USA), respectively. In Model  
90 42C-TL trace-level chemiluminescent analyser, NO<sub>2</sub> is converted to NO by a molybdenum NO<sub>2</sub>-to-NO converter heated to  
about 325°C. The converter efficiency was checked annually using gas phase titration (GPT). If the converter efficiency is less  
than 96%, replace the converter. Data are recorded as 5 min averages. The meteorological parameters (WS, wind direction, T,  
and RH) for a given period were obtained from the routine meteorological observations at the station. The main objective of  
operational observations of reactive gases at regional background stations is to obtain accurate trends in the measured reactive

95 gases, for which reliable and comparable data are essential. Therefore, strict quality control measures were implemented during the observation process (Lin et al., 2019). The quality control measures mainly included the following: (1) daily zero and span checks (automatic); (2) monthly multi-point calibrations ( $\geq 5$  points, including zero); (3) comparisons of reference  $\text{SO}_2/\text{N}_2$  and  $\text{NO}/\text{N}_2$  gas mixtures to the standards of the National Institute of Standards and Technology before and after their usage (periodically) to ensure data traceability; (4) instrument self-diagnosis, manual testing, checking, and maintenance (US EPA, 100 2017); and (5) data correction according to the quality control results, especially the results of zero/span checks and multipoint calibrations.

From 1 January 2006 to 31 December 2016, a total of 93,759 and 90,453 valid hourly average data points were obtained for  $\text{NO}_x$  and  $\text{SO}_2$ , respectively. Missing data totalled 2673 h and 5979 h for  $\text{NO}_x$  and  $\text{SO}_2$ , respectively. The missing  $\text{NO}_x$  data were mainly for the period from 2 to 13 February 2007 and from 24 July to 8 October 2012. The missing  $\text{SO}_2$  data were mainly 105 for the period from 23 September to 21 December 2013, from 8 to 26 May 2014, and from 17 October 2014 to 24 January 2015.

### 2.3 Data processing methods

(1) Data statistics. The daily means of  $\text{NO}_x$  and  $\text{SO}_2$  were calculated using the hourly average data, and only daily mean data calculated from at least 18 hourly data were used as valid daily means. The monthly means of  $\text{NO}_x$  and  $\text{SO}_2$  were calculated 110 from the valid daily average data and considered valid if they were based on at least 21 valid daily averages (or at least 17 valid daily averages in February). Annual means were calculated on the basis of the complete monthly mean data each year. If a month's mean data were unavailable, we used an interpolating value from the corresponding monthly means in different years during the observation. In China, spring is from March to May, summer is from June to August, autumn is from September to November, and winter is from December to February.

115 (2) Monthly satellite based  $\text{NO}_2$  OMI data were provided by Lin's research group at Peking University; the data were retrieved using an optimized inversion algorithm (Lin et al., 2014; Lin et al., 2015; Boersma et al., 2019). A grid range of  $115.125^\circ \text{E}$ – $122.875^\circ \text{E}$  and  $27.125^\circ \text{N}$ – $35.875^\circ \text{N}$  was selected to cover the entire YRD region.

### 2.4 Concentration weighted trajectory method

We used the concentration weighted trajectory (CWT) method to identify potential source areas (PSAs) of  $\text{NO}_x$  and  $\text{SO}_2$  120 because this method can effectively distinguish the relative strength of potential sources (Xin et al., 2016). In the CWT method, the study area is divided into  $i \times j$  small grids with equal size, and each grid ( $i, j$ ) is assigned a weighted concentration according to the following equation:

$$C_{ij} = \frac{1}{\sum_{k=1}^m \tau_{ijk}} \sum_{k=1}^m C_k \tau_{ijk} \quad (1)$$

125 Where  $k$  denotes the indicator of a trajectory,  $m$  denotes the total number of trajectories,  $C_k$  denotes the concentration observed when trajectory  $k$  arrives, and  $\tau_{ijk}$  is the residence time of trajectory  $k$  in the  $ij_{th}$  grid cell. To reduce errors in the more distant grids, an empirical weighting factor  $W_{ij}$  is introduced (Wang et al., 2006; Deng et al., 2020), with the following equation:

$$CWT(i,j) = W_{ij} \times C_{ij} \quad (2)$$

130

$$W_{ij} = \begin{cases} 1 & (n_{i,j} > 3n_{ave}) \\ 0.7 & (3n_{ave} < n_{i,j} < 1.5n_{ave}) \\ 0.42 & (1.5n_{ave} < n_{i,j} < n_{ave}) \\ 0.05 & (n_{i,j} < n_{ave}) \end{cases} \quad (3)$$

Here,

$$n_{ave} = \frac{D \times t \times n}{i \times j} \quad (4)$$

Where  $D$  denotes the number of days included,  $t$  denotes the number of trajectories per day,  $n$  denotes the trajectory endpoints of each trajectory, and  $i \times j$  denotes the total number of grids.

135 We used a hybrid single-particle Lagrangian integrated trajectory model (Hysplit4.9) from National Oceanic and Atmospheric Administration, USA, to calculate the 24-h backward trajectories at 10 m above ground level over LAN during 2006–2016; the NCEP–NCAR reanalysis meteorological data set (<https://ready.arl.noaa.gov/archives.php>) and was used to calculate the trajectories and atmospheric mixed layer heights. The computed backward trajectories were subsequently processed using the TrajSat plug-in for CWT in Meteoinfo software (Wang, 2014), covering the region located within 20–40° N and 110–130° E  
140 and with a grid size resolution of 0.5° × 0.5°.

### 3 Results and discussion

#### 3.1 Observational levels and comparison with other sites

The hourly average  $NO_x$  mixing ratios at LAN ranged from 0.4 ppb to 165.6 ppb, with  $NO_2$  mixing ratios ranging from 0.2 ppb to 106.8 ppb. Only 3 hours' data exceeded the secondary standard limit value for  $NO_2$  (106 ppb) as stated in the national  
145 ambient air quality standard (GB3095–2012). The hourly average  $SO_2$  mixing ratios ranged from 0.1 ppb to 128.6 ppb, which were all below the GB3095–2012 secondary standard limit for  $SO_2$  (190 ppb).

Table 1 presents annual statistics of the  $NO_2$ ,  $NO_x$  and  $SO_2$  mixing ratios observed at LAN between 2006 and 2016. The overall average mixing ratios with  $\pm 1$  standard deviation of for  $NO_x$  ( $NO_2$ ) and  $SO_2$  from 2006 to 2016 were  $13.6 \pm 1.2$  ppb ( $12.5 \pm 4.6$  ppb) and  $7.0 \pm 4.2$  ppb, respectively, with the highest  $NO_x$  ( $NO_2$ ) value being observed in 2012 and the highest  $SO_2$   
150 in 2006.  $NO_2$  was the dominant form of  $NO_x$ , accounting for 82.2 % of  $NO_x$  (according to the slope value from the reduced major axis regression on hourly average  $NO_2$  and  $NO_x$  data). The average  $NO_2$  mixing ratio was  $12.5 \pm 4.6$  ppb, which was below the primary annual limit of 21.2 ppb in GB 3095–2012. Some information on  $NO_2(NO)$  can be seen the supplementary

material (Tab.S1). The average SO<sub>2</sub> mixing ratio from 2006 to 2016 is close to the primary annual limit of 7.6 ppb in GB3095–2012. However, the annual average SO<sub>2</sub> mixing ratios (10.6–14.6 ppb) from 2006 to 2008 was much higher than the limit of the primary standard though lower than the limit of the secondary standard (22.8 ppb).

Table 2 compares the levels of NO<sub>x</sub> and SO<sub>2</sub> mixing ratios at LAN with those corresponding SO<sub>2</sub>/NO<sub>x</sub> ratios at other background stations in seven geographic regions of China: north, east, south, northeast, northwest, southwest, and central China. The NO<sub>x</sub> mixing ratio at LAN was slightly higher than that at Shangdianzi (12.7 ± 11.8 ppb) in northern China, equal to that at Dinghushan (13.6 ppb) in southern China, and much higher than those at Wuyishan (2.70 ppb) in eastern China, Fukang (8.3 ppb) in northwest China, Changbai Mountain (4.7 ppb) in northeast China, Jinsha (5.6 ± 5.5 ppb) in central China, and Southwest Gongga Mountain (0.90 ppb). These results indicate that LAN recorded the highest level of NO<sub>x</sub> among the regional atmospheric background stations in China, which could be attributed to the developed economy of the YRD region. The SO<sub>2</sub> mixing ratio at LAN was close to that at Shangdianzi (7.6 ± 10.2 ppb) in northern China, higher than that at Dinghu Mountain (6.5 ppb) in southern China, and much higher than those at Wuyishan (1.48 ppb) in eastern China, Changbai Mountain (2.1 ppb) in northeast China, Fukang (2.2 ppb) in northwest China, Gongga Mountain (0.19 ppb), and Jinsha (2.8 ± 5.5 ppb) in central China. The regional difference in NO<sub>x</sub> and SO<sub>2</sub> was closely related to the diverse levels of economic development in China's regions because it was broadly characterised by a higher level in the eastern than in central and western regions. The SO<sub>2</sub>/NO<sub>x</sub> ratio at LAN was at a high level in China, which reflects the different energy structures to some extent.

### 3.2 Seasonal variations

Figure 3 illustrates the average seasonal variations in NO<sub>x</sub> and SO<sub>2</sub> mixing ratios at LAN. The maximum monthly average mixing ratios of NO<sub>x</sub> and SO<sub>2</sub> were observed in December and January, at 23.5 ± 4.4 ppb and 11.9 ± 6.2 ppb, respectively. The minimum values both occurred in July, at 7.1 ± 0.8 ppb and 2.8 ± 2.3 ppb, respectively. The average monthly variations in NO<sub>x</sub> exhibited significant correlations with the monthly NO<sub>2</sub> satellite data ( $R^2 = 0.82$ ,  $P < 0.001$ ). Seasonal variation patterns of NO<sub>x</sub> and SO<sub>2</sub> look alike, showing a concave shape with its minimum in summer. The highest mixing ratios occurred in winter (NO<sub>x</sub>: 19.5 ppb; SO<sub>2</sub>: 10.1 ppb), followed by spring (NO<sub>x</sub>: 13.4 ppb; SO<sub>2</sub>: 7.8 ppb), autumn (NO<sub>x</sub>: 13.6 ppb; SO<sub>2</sub>: 6.7 ppb), and summer (NO<sub>x</sub>: 8.1 ppb; SO<sub>2</sub>: 3.3 ppb). The monthly average mixing ratios of both NO<sub>x</sub> and SO<sub>2</sub> showed a dip in February—a phenomenon also observed in NO<sub>x</sub> and SO<sub>2</sub> (Wang et al., 2016; Xue et al., 2020) and NO<sub>3</sub><sup>-</sup> and SO<sub>4</sub><sup>2-</sup> in PM<sub>2.5</sub> in Shanghai (Duan et al., 2020). The source emission inventory data indicated that NO<sub>x</sub> and SO<sub>2</sub> emissions from industry, transportation, and coal-fired power plants were all lower in February than in January and March throughout China (Li et al., 2017), which may be related to decreased emissions due to lower economic activity during Chinese Spring Festival. In addition, the higher RH in February (Fig. 2) might have led to higher NO<sub>x</sub> and SO<sub>2</sub> removal rates.

### 3.3 Diurnal variations

Figure 4 shows the annual and seasonal average diurnal variations in NO<sub>x</sub> and SO<sub>2</sub> at LAN from 2006 to 2016, along with the annual average diurnal variations in NO<sub>x</sub> and SO<sub>2</sub> at some other sites in the YRD. The overall diurnal profile of NO<sub>x</sub> displayed

185 a double-peak and double-valley pattern (Fig. 4a). The valley values occurred at 05:00–06:00 and 13:00, with mixing ratios of 12.3 ppb and 10.0 ppb, respectively, and the peak values occurred at 09:00 and 19:00, with mixing ratios of 13.1 ppb and 14.4 ppb, respectively. Surrounding areas, such as Chongming, Pudong (Xue et al., 2020), and Xujiahui (Gao et al., 2017) in Shanghai City, Hangzhou (Zhou et al., 2020) in Zhejiang Province, and Nanjing (Wang et al., 2017) in Jiangsu Province also exhibited a double-peak and double-valley type of average diurnal variation in NO<sub>x</sub> (Fig. 4a), indicating a regional NO<sub>x</sub> 190 pollution characteristic. However, at most atmospheric background stations, the average diurnal variations in NO<sub>x</sub> exhibited a single-peaked and single-valley pattern, such as those at Xinglong in north China (Yang et al., 2012), Tianhu in the Pearl River Delta (Shen et al., 2019), Dae Hung in South Korea (Pandey et al., 2008), and Mount Cimone in Italy (Cristofanelli et al., 2016), suggesting a more complex anthropogenic influence in the YRD region. In summer, the seasonal average diurnal variation in NO<sub>x</sub> showed a morning peak at 08:00, which time is 1 to 2 h earlier than that occurred in other seasons (Fig. 4c). 195 SO<sub>2</sub> at LAN showed relatively small average diurnal variation (Fig. 4b), with higher mixing ratios from midnight to noontime and lower ones during later afternoon and evening. The average diurnal amplitude of SO<sub>2</sub> at LAN was much smaller than those found in Nanjing and Jiaxing. The seasonal average diurnal profiles of SO<sub>2</sub> at LAN were similar to the annual average one except for that in winter, which had a peak around noon (Fig. 4d).

The diurnal variation of pollutants emitted at ground level are closely related to the intensity of emissions, atmospheric 200 transport, diurnal development in boundary layer height, and atmospheric photochemical reactions (Resmi et al., 2020). The mixing layer depth (MLD) was much lower at night than during the daytime, as shown in Fig. 4b. Low MLDs at night are not conducive to pollutant dispersion, whereas high MLDs during the daytime are conducive to pollutant dispersion. This day-night difference in the MLD is one of the factors causing lower levels of SO<sub>2</sub> and NO<sub>x</sub> during afternoon hours. Photochemistry during the daytime also contributes to rapid chemical transformation of SO<sub>2</sub> and NO<sub>x</sub>, which results in low NO<sub>x</sub> and SO<sub>2</sub> 205 mixing ratios in the afternoon. Overall, the morning peak of NO<sub>x</sub> was lower than the evening peak, the morning peak of SO<sub>2</sub> was higher than the evening subpeak, and the morning peak of SO<sub>2</sub> was not as protruding as and occurred slightly later than that of NO<sub>x</sub>, reflecting the differences in their sources. The morning peak of NO<sub>x</sub> may be influenced by vehicle emissions during the morning rush hour, and the early peak of SO<sub>2</sub> may be more influenced by vertical changes during the developing mixed layer depth height (Qi et al., 2012). The evening peaks of NO<sub>x</sub> and SO<sub>2</sub> were relatively similar because both were 210 closely related to the MLD decrease and for NO<sub>x</sub> likely also vehicle emissions during the evening rush hour.

### 3.4 Influence of meteorological factors

Changes in meteorological factors have considerable effects on the levels of air pollutants. In this section, we investigate the influences of meteorological factors on the variations in NO<sub>x</sub> and SO<sub>2</sub> mixing ratios through statistical plots showing relationships between pollutant concentrations and meteorological factors as well as correlation analysis. The variation 215 characteristics of hourly average mixing ratios of NO<sub>x</sub> and SO<sub>2</sub> along with meteorological parameters are presented in Fig. 5. The data are grouped into three subsets corresponding to time periods: I (2006–2009), II (2010–2013) and III (2014–2016).

The variation characteristics of  $\text{NO}_x$  and  $\text{SO}_2$  with WS (Fig. 5a,b) were consistent during period I, showing decreases of  $\text{NO}_x$  and  $\text{SO}_2$  with increasing WS. Higher WS facilitated the dilution of  $\text{NO}_x$  and  $\text{SO}_2$  and vice versa. However, the situation for  $\text{SO}_2$  was different during period II and III, when the  $\text{SO}_2$  level was stable with the change of WS. The correlation of T between the two pollutants varied considerably, with the  $\text{SO}_2$  mixing ratios decreasing nearly monotonically with increasing T (Fig. 5d), whereas  $\text{NO}_x$  increased with increasing T in the low temperature range and decreased with increasing T in the high temperature range (Fig. 5c). Fig. 5c indicates a positive correlation between  $\text{NO}_x$  and T in winter and negative correlations in other seasons, but the positive correlation in winter is weak and insignificant (Table 3). Pandey et al. (2008) reported that low T might facilitate the increase of  $\text{NO}_x$  emissions from motor vehicle exhaust. The variations in  $\text{NO}_x$  and  $\text{SO}_2$  with RH (Fig. 5e,f) exhibit a convex pattern and the former patterns in 3 different periods are well consistent but the latter ones are not at low RH. The correlation between  $\text{SO}_2$  and RH was stronger than that of  $\text{NO}_x$  and RH (Table 3). The variation characteristics of  $\text{NO}_x$  and  $\text{SO}_2$  mixing ratios with the MLD exhibited diverse patterns (Fig. 5g,h). The mixing ratio of  $\text{NO}_x$  decreased with increasing MLD. However, the  $\text{SO}_2$  levels during period II and III remained nearly stable in the whole MLD range and a slight decline of  $\text{SO}_2$  with increasing MLD was only observed during period I. The difference in  $\text{NO}_x$  and  $\text{SO}_2$  mixing ratios with the MLD implies that the  $\text{NO}_x$  sources mostly impacting the LAN site should be mainly in the near-surface layer, such as emissions from motor vehicles and small burners, whereas  $\text{SO}_2$  may originate from the vertical exchange of elevated sources transported in the higher altitude layer (200–1300 m).

Figure 6 displays the rose diagrams of  $\text{NO}_x$  and  $\text{SO}_2$  mixing ratios in different seasons. There are some seasonal differences in the dependence of  $\text{NO}_x$  and  $\text{SO}_2$  on wind direction. In summer, the high mixing ratios of  $\text{NO}_x$  and  $\text{SO}_2$  were mainly from the NW–NNE and SSW–NW sectors, respectively (Fig. 6b). In other seasons, relatively high  $\text{NO}_x$  and  $\text{SO}_2$  values were mainly from the N–ENE and S–WSW directions, respectively, under the influences of the dominant and subdominant WDs (Fig. 2b, d). Overall,  $\text{NO}_x$  and  $\text{SO}_2$  observed at LAN originated mainly from the NW-ENE and SSW-NW sectors, respectively. However, this result provides only little information about the actual geographic distributions of major  $\text{NO}_x$  and  $\text{SO}_2$  sources influencing LAN. Therefore, we used the CWT method to identify the PSAs for  $\text{NO}_x$  and  $\text{SO}_2$ . Fig. 7 presents the areas, from which  $\text{NO}_x$  and  $\text{SO}_2$  observed at LAN originated. Although the PSAs covered the entire YRD, the PSAs for the highest  $\text{NO}_x$  and  $\text{SO}_2$  levels appeared mainly in the eastern coastal region, which is closely related to the booming local economy. More obvious provincial differences were observed in a higher PSA for  $\text{NO}_x$  than that for  $\text{SO}_2$ . Temporally, the high PSA (>10 ppb) of  $\text{NO}_x$  and  $\text{SO}_2$  was most extensive in winter, followed by spring and autumn, with the least extensive PSA in summer. The  $\text{NO}_x$  PSAs over coastal areas were more extensive than those for  $\text{SO}_2$  in each season. The YRD is one of the five major port clusters in China; thus, this region's ship emissions might be a major cause of this difference (Fan et al., 2016; Wan et al., 2020). The CWT analysis indicated that  $\text{SO}_2$  was mainly influenced by industrial emissions from inland areas, whereas  $\text{NO}_x$  was mainly influenced by both inland and marine traffic.

### 3.5 Long-term variations in NO<sub>x</sub> and SO<sub>2</sub> mixing ratios

Fig. 8 displays the variations in the annual and seasonal average NO<sub>x</sub> and SO<sub>2</sub> mixing ratios observed at LAN during 2006-2016, together with estimated annual emissions in the YRD. The annual average of NO<sub>x</sub> showed an increase followed by a decrease, while that of SO<sub>2</sub> experienced a nearly monotonic decrease. The annual NO<sub>x</sub> mixing ratio revealed an increase, with a rate of +0.31 ppb/yr ( $R^2 = 0.28$ ,  $P = 0.16$ ) during 2006–2011 and a significant decreasing trend, with a rate of –0.78 ppb/yr or –5.16 %/yr ( $R^2 = 0.85$ ,  $P < 0.01$ ) during 2011–2016 (Fig. 8a). The decreasing rate was less than that found in urban Shanghai (2.1 ppb/yr; Gao et al., 2017). Selecting 2006 as the base year, we compared the annual percentage change in NO<sub>x</sub> at LAN (0.49 %/yr) during 2006–2016 with those of other regions over the same period. The *Ecological and Environmental Status Bulletin* (Shanghai Municipal Bureau of Ecology and Environment, 2007–2017; Department of Ecology and Environment of Zhejiang Province, 2007–2017; Department of Ecology and Environment of Jiangsu Province, 2007–2017) reported a similar change of –0.45 %/yr in the YRD region (without data for Anhui Province), reflecting the suitable regional representativeness of LAN. The annual percentage decrease of NO<sub>x</sub> at LAN and in the YRD was much smaller than those in many regions—for example, the Pearl River Delta in China (–2.84 %/yr; Yan et al., 2020), Kraków City in Poland (–2.21%/yr; Agnieszka and Gruszecka-Kosowska, 2020), at Preila station in Lithuania (–1.60 %/yr; Davulienė et al., 2021), and in New York City in the United States (–3.46 %/yr; Squizzato et al., 2018)—but more favourable than those in some other regions, such as Wuhan City in China (+2.08 %/yr; Li et al., 2020) and Amersfoort City (+6.50 %/yr) and Louis Trichardt City in South Africa (+1.85 %/yr; Swartz et al., 2020b). Compared with other background regions in China, the annual change of NO<sub>x</sub> at LAN was less favourable than that in north China (–3.34 %/yr) with a base year of 2005 (Bai et al., 2015) and more favourable than that in northwest China (+12.98 %/yr) with a base year of 2010 (Li et al., 2019).

Figure 8 also presents the NO<sub>x</sub> emission data from the *China Ecological Environment Bulletin* in different years. The change of the annual average NO<sub>x</sub> mixing ratio was highly correlated with the total NO<sub>x</sub> emissions ( $R^2 = 0.92$ ,  $P < 0.001$ ) and total industrial emissions ( $R^2 = 0.94$ ,  $P < 0.001$ ) in the YRD region. The peak surface NO<sub>x</sub> mixing ratio was observed in 2011. Since China began to control and reduce NO<sub>x</sub> emissions as part of the *12th Five-Year Plan* (2011–2015) and promulgated the strict *Air Pollution Prevention and Control Action Plan* in 2013, many flue gas denitrification systems have been installed in coal-fired power plants and heavy industry operations (Zhao et al., 2019), resulting in a decrease in annual NO<sub>x</sub> emission since 2011. The seasonal long-term trends of NO<sub>x</sub> did always resemble the annual trend. While seasonal NO<sub>x</sub> mixing ratios in winter, autumn, and spring increased before 2011 and then decreased, just like the annual NO<sub>x</sub> mixing ratio did, the seasonal NO<sub>x</sub> mixing ratio in summer exhibited a nearly monotonic decreases from 2006 to 2016 at 0.11 ppb/yr ( $R^2 = 0.20$ ,  $P = 0.09$ ) (Fig. 8c). Regarding the seasonal linear fitting trends, the highest increasing and declining trends were observed in winter (+1.29 ppb/ yr,  $R^2 = 0.52$ ,  $P = 0.06$ ; –2.33 ppb/yr,  $R^2 = 0.94$ ,  $P < 0.01$ ), followed by autumn (+1.24 ppb/yr,  $R^2 = 0.65$ ,  $P = 0.02$ ; –0.41 ppb/yr,  $R^2 = 0.12$ ,  $P = 0.30$ ) and spring (+0.31 ppb/yr,  $R^2 = 0.93$ ,  $P < 0.001$ ; –1.16 ppb/yr,  $R^2 = 0.76$ ,  $P = 0.09$ ). We found a significant correlation ( $P < 0.05$ ) between surface NO<sub>2</sub> mixing ratio and OMI NO<sub>2</sub> vertical column density over YRD (Fig. S3b). To better compare the changes in the two over the same period, we have fitted a linear fit to the data from 2006 to 2011

and from 2011 to 2016 respectively (Fig.S3a). The surface and the OMI NO<sub>2</sub> increased at 2.23%/yr ( $R^2 = 0.264$ ,  $P = 0.17$ ) and 5.87%/yr ( $R^2 = 0.855$ ,  $P < 0.01$ ) (based on 2006), respectively, during the up period and decreased at -4.98%/yr ( $R^2 = 0.823$ ,  $P < 0.01$ ) and -4.22%/yr ( $R^2 = 0.897$ ,  $P < 0.01$ ), respectively, during the declining period.

Annual mean SO<sub>2</sub> mixing ratios revealed a significant decreasing trend (-0.99 ppb/yr,  $R^2 = 0.92$ ,  $P < 0.001$ ) during 2006-2016 (Fig. 8b). The annual decreasing rate of SO<sub>2</sub> at LAN (-8.27 %/yr) was more rapid than those in the whole YRD (-6.65 %/yr), in the background area in north China (-0.78 %/yr; Bai et al., 2015), and in northwest China (-5.4 %/yr; Li et al., 2019). Different from NO<sub>x</sub>, the annual average of SO<sub>2</sub> at LAN decreased more rapidly than in most of the aforementioned regions (Table 4), which demonstrates the effectiveness of the policies in controlling SO<sub>2</sub> emission during the observation period in the YRD.

The change in the annual SO<sub>2</sub> mixing ratio was closely correlated with changes in industrial SO<sub>2</sub> emission ( $R^2 = 0.95$ ,  $P < 0.001$ ) and total SO<sub>2</sub> emission ( $R^2 = 0.94$ ,  $P < 0.001$ ) in the YRD (Fig. 8b). In 2011, the SO<sub>2</sub> mixing ratio rebounded slightly, with an increase of 9 % compared with the value in 2010. This seemed to be consistent with the variation of industrial SO<sub>2</sub> emission. The weakening impact of the global financial crisis and the recovery of industry in the YRD region may explain this slight rebound in SO<sub>2</sub> emissions (Xie, 2017b). Seasonally, the SO<sub>2</sub> mixing ratio exhibited the strongest decreasing trend (-1.69 ppb/yr,  $R^2 = 0.90$ ,  $P < 0.001$ ) in winter, followed by spring (-1.05 ppb/yr,  $R^2 = 0.97$ ,  $P < 0.001$ ) and autumn (-0.99 ppb/yr,  $R^2 = 0.93$ ,  $P < 0.001$ ), with the smallest decreasing trend observed in summer (-0.35 ppb/yr,  $R^2 = 0.61$ ,  $P < 0.001$ ).

In the annual statistics, the 95th and 5th percentile of the pollutants' concentrations can be regarded as influenced by polluted and clean air masses, respectively. The annual trends of the 95th percentile of NO<sub>x</sub> and SO<sub>2</sub> (Fig. 9a) exhibited similar patterns to the corresponding trends in annual average mixing ratios (Fig. 8a, b), but the peak of the 95th percentile of NO<sub>x</sub> occurred in 2012, instead of in 2011. Hao and Song (2018) noted that the NO<sub>x</sub> emissions from vehicles peaked in Hangzhou and Ningbo in 2012, which may explain the peak of the 95th percentile occurring later than that in the annual data. Moreover, the 95th percentile of the SO<sub>2</sub> mixing ratio decreased at a remarkable rate (-8.9 ppb/yr) from 2007 to 2009, which is approximately 2.8 times as strong as the overall rate of decrease during the 11-year period (-3.2 ppb/yr). Substantial decreases were also found in the 95th percentiles of the CO mixing ratio (Chen et al., 2020) and the NO<sub>x</sub> mixing ratio from 2007 to 2009 at LAN. It is highly possible that this phenomenon was caused by reduced industrial productions and related emissions following the 2008 global financial crisis. As displayed in Fig. 9b, the level of NO<sub>x</sub> in cleaner air mass arriving at LAN exhibited an increasing trend, with a rate of +0.17 ppb/yr, from 2006 to 2014 ( $R^2 = 0.86$ ,  $P < 0.001$ ) and then declined after 2014. This is inconsistent with the trend of the 95th percentile of the NO<sub>x</sub> mixing ratio, suggesting the polluted and relative clean air masses arriving at LAN were impacted by different emission sources of NO<sub>x</sub>. Interestingly, the 5th percentile of the NO<sub>x</sub> level was significantly correlated ( $R^2 = 0.74$ ,  $P < 0.001$ ) with the road emissions of NO<sub>2</sub> in the YRD (Kurokawa and Ohara, 2020), suggesting that the lower end of NO<sub>x</sub> mixing ratios was mainly determined by long-range transported background air containing NO<sub>x</sub> from road emissions, while the high end was mainly associated with emissions from industrial production as well as power generation. The level of SO<sub>2</sub> in cleaner air mass exhibited a decreasing trend at a rate of -0.2 ppb/yr ( $R^2 = 0.61$ ,  $P < 0.01$ ).

Figure 10 displays the scatter plot of the daily average SO<sub>2</sub> and NO<sub>x</sub> mixing ratio during period I, II and III at LAN. Reduced major axis regressions were performed on three data subsets. The daily mean mixing ratios of NO<sub>x</sub> were significantly ( $R^2 = 0.29$ ,  $P < 0.001$ ) and positively correlated with those of SO<sub>2</sub>. The ratios of SO<sub>2</sub> to NO<sub>x</sub> (SO<sub>2</sub>/NO<sub>x</sub>) were 0.96, 0.53, and 0.33 (slopes in the regression lines) during period I, II and III, respectively. The decreasing SO<sub>2</sub>/NO<sub>x</sub> suggests that SO<sub>2</sub> emissions were more efficiently reduced than NO<sub>x</sub> emissions. Such a change in emission ratio not only affected ambient SO<sub>2</sub>/NO<sub>x</sub> but also the ratios of sulphate/nitrate in PM<sub>2.5</sub> in Shanghai from 2009 to 2012 (Zhao et al., 2015) SO<sub>4</sub><sup>2-</sup>/NO<sub>3</sub><sup>-</sup> in rainwater in Hangzhou (Yang, 2018; Xu et al., 2019). These results indicate that NO<sub>x</sub> has been gaining a more important role in the processes of precipitation acidification and secondary inorganic aerosol formation in the YRD region. Therefore, NO<sub>x</sub> emission reduction should be further strengthened in subsequent air pollution control measures and legislation in the YRD region.

Figure 11 reveals the average diurnal variations in NO<sub>x</sub> and SO<sub>2</sub> during the period I, II and III. During these three periods, the average diurnal curves in NO<sub>x</sub> exhibited a valley around 13:00, with minimum values of 7.5 ppb, 11.2ppb, and 9.2 ppb, respectively. The morning and evening NO<sub>x</sub> peaks, which occurred respectively at 09:00 and 19:00, became increasingly distinct over time (Fig. 11a, c, e). The morning and evening peak NO<sub>x</sub> values were 9.8 ppb and 10.9 ppb during period I, 14.6 ppb and 15.8 ppb during period II, and 12.3 ppb and 13.6 ppb during period III. The gradual protruding of the morning and evening peaks should be mainly caused by increasing vehicle emissions during the morning and evening rush hours. According to the 2010 Annual Report on China's Motor Vehicle Pollution Prevention and Control, the state introduced a series of policies to promote automobile and motorbike ownership in response to the international financial crisis and to ensure economic growth; these policies effectively stimulated the automobile market (Mi and Qin, 2011; Hao and Song, 2018) and led to an increase in vehicle emissions and atmospheric oxidation in the YRD region (Yu et al., 2019). Thus, the NO<sub>x</sub> mixing ratios around the morning and evening peaks were much higher than those at night during period II (Fig. 11e), which differs much from the pattern during period I (Fig. 11a). The disappearance of the small peak around 01:00 at night during 2012–2016 may be related to the introduction of stricter air pollution control policies for factories that emit at night. Small peaks in NO<sub>x</sub> and SO<sub>2</sub> occurred between 01:00 and 02:00, which might be related to nighttime emissions from unscrupulous enterprises (Fan et al., 2013) or more production activities with lower electricity prices after midnight in response to the financial pressure of the 2008 economic crisis and the corresponding increase in electricity prices for industrial users (Sun, 2008). In spite of these two reasons, however, it's really hard to tell exactly why these small peaks dominate after midnight.

The average diurnal variation curve of SO<sub>2</sub> at LAN period I (Fig. 11b) is of the single-valley type, with an average valley mixing ratio of 6.5 ppb. After 2010, the peak shape has changed from single-valley type to the double-peak and double-valley type (Fig. 11d, f). The valleys of SO<sub>2</sub> during period II occurred at 06:00 and 15:00, with average mixing ratios of 5.2 ppb and 4.7 ppb, and the peaks occurred at 10:00 and 19:00, with average mixing ratios of 5.9 ppb and 5.3 ppb, respectively. The NO<sub>x</sub> and SO<sub>2</sub> evening peaks occurred at the same time (19:00), but the SO<sub>2</sub> morning peak time was 1 hour later than the NO<sub>x</sub> morning peak (09:00), indicating that the NO<sub>x</sub> and SO<sub>2</sub> morning peaks were influenced by different sources, whereas the evening peaks were from similar sources. The formation of the SO<sub>2</sub> morning peak may be mainly related to the vertical

exchange during the development of the atmospheric boundary layer and the air in the upper layer with a higher SO<sub>2</sub> mixing ratio than that at the surface draining down. The formation of the evening peaks of NO<sub>x</sub> and SO<sub>2</sub> may be mainly related to the increase in motor vehicle and residential sources emissions, which are stronger in the rush and cooking hours and that of SO<sub>2</sub> may be probably more due to the reduction of power plants emissions. Compared with that during period II, the SO<sub>2</sub> mixing ratios at the morning and evening peaks in period III were approximately 3 ppb lower, suggesting that the large emitters that release SO<sub>2</sub> all the time were emitting less and less.

## Conclusions

In this study, we characterized the seasonal and diurnal variations and analysed the long-term trends in NO<sub>x</sub> and SO<sub>2</sub> mixing ratios in the YRD background area during the period of 2006–2016. We also tried to understand the variations and trends in terms of the changes in emissions and meteorological conditions. The hourly average mixing ratios of NO<sub>x</sub> (NO<sub>2</sub>) and SO<sub>2</sub> at the LAN background station varied in the ranges of 0.4–165.6 ppb (0.2–106.8 ppb) and 0.1–128.6 ppb, respectively. The levels of NO<sub>x</sub> and SO<sub>2</sub> were highest in winter, followed by spring and autumn, and lowest in summer. Although a significant correlation was observed between the daily average mixing ratios of NO<sub>x</sub> and SO<sub>2</sub> ( $R^2 = 0.29$ ,  $P < 0.001$ ), their average diurnal variation characteristics differed from each other, with morning peaks in SO<sub>2</sub> occurring later than in NO<sub>x</sub>.

The annual average mixing ratio of NO<sub>x</sub> (NO<sub>2</sub>) fluctuated upwards between 2006 and 2011 (+0.31 ppb/yr,  $P = 0.16$ ) (+0.27 ppb/yr,  $P = 0.17$ ) with a mean value of 13.8 ppb and then began to decrease significantly from 2011 to 2016 (–0.78 ppb/yr,  $P < 0.01$ ) (–0.70 ppb/yr,  $P < 0.01$ ), with a mean value of 13.7 ppb (12.5 ppb). The annual average mixing ratio of NO<sub>x</sub> was significantly correlated with the industrial ( $R^2 = 0.88$ ,  $P < 0.001$ ) and total ( $R^2 = 0.86$ ,  $P < 0.001$ ) NO<sub>x</sub> emissions in the YRD, so as between surface and OMI NO<sub>2</sub> (Fig.S3b,  $R^2=0.61$ ,  $P < 0.01$ ). The annual 95 % percentile of NO<sub>x</sub> mixing ratios followed a similar trend to the annual average, whereas the 5th percentile levels fluctuated upwards at +0.17 ppb/yr from 2006 to 2014, reflecting the increasing regional background level of NO<sub>x</sub> in the YRD during those years, which was related to the continued increase in vehicle numbers in the YRD. The annual average mixing ratio of SO<sub>2</sub> exhibited a rapid and significant decreasing trend (–0.99 ppb/yr,  $P < 0.001$ ) and was closely correlated to total SO<sub>2</sub> emission ( $R^2 = 0.94$ ,  $P < 0.001$ ) and total SO<sub>2</sub> industrial emission ( $R^2 = 0.95$ ,  $P < 0.001$ ) in the YRD. The reduced emissions were resulted from the strong and effective introduction of national control policies. The yearly decrease of SO<sub>2</sub>/NO<sub>x</sub> ratios suggest a more effective reduction in SO<sub>2</sub> than in NO<sub>x</sub>. Thus, NO<sub>x</sub> emission control needs to be further strengthened in the future.

We found gradual changes in diurnal patterns of both gases. After 2010, both NO<sub>x</sub> and SO<sub>2</sub> showed diurnal patterns with two peaks and two valleys. The morning peak of NO<sub>x</sub> occurred at approximately 09:00, earlier than that of SO<sub>2</sub> (10:00), and the evening peak occurred at the same time as SO<sub>2</sub> (19:00). The morning and evening peaks of both gases protruded gradually. This phenomenon can hardly be attributed to changes in meteorological conditions (such as the MLD). We believe that changes in major sources of NO<sub>x</sub> and SO<sub>2</sub> should be the cause, with increasing NO<sub>x</sub> emission from vehicles resulting in higher NO<sub>x</sub>

peaks during rush hours and reduced SO<sub>2</sub> emissions from power plants and other large point sources making the SO<sub>2</sub> peaks  
380 relatively protruding.

**Data availability.** The data of stationary measurements are available upon request to the contact author Weili Lin  
(linwl@muc.edu.cn).

**Author contributions.** QY wrote the paper, WL and XX developed the idea f, formulated the research goals, and edit the paper.  
385 QM and JY carried out the measurement of NO<sub>x</sub> and SO<sub>2</sub> and analysed the meteorological data.

**Competing interests.** The authors declare that they have no conflict of interest.

### Acknowledgements.

This study was funded by the National Natural Science Foundation of China (Grant No. 91744206).

### References

- 390 Agnieszka, P. T., and Gruszecka-Kosowska: The Condition of Air Pollution in Kraków, Poland, in 2005–2020, with Health Risk Assessment,  
Int. J. Env. Res. Pub. He., 17, E6063, <https://doi.org/10.3390/ijerph17176063>, 2020.
- Bai, J., Wu, J., Chai, W., Wang, P., and Wang, G.: Long-Term Variation of Trace Gases and Particulate Matter at an Atmospheric  
Background Station in North China, Forn.Earth Sci., 248–263, <https://doi.org/10.12677/ag.2015.53025>, 2015.
- Chen, L.: Measure and Study on the Atmospheric Pollutants in Three Typical Regional Background Stations of China, Lanzhou University,  
395 2012.
- Chen, Y., Ma, Q., Lin, W., Xu, X., Yao, J., and Gao, W.: Measurement report: Long-term variations in carbon monoxide at a background  
station in China’s Yangtze River Delta region, Atmos. Chem. Phys., 20, 15969–15982, <https://doi.org/10.5194/acp-20-15969-2020>, 2020.
- Cheng, L., Ji, D., He, J., Li, L., Du, L., Cui, Y., Zhang, H., Zhou, L., Li, Z., and Zhou, Y.: Characteristics of air pollutants and greenhouse  
gases at a regional background station in Southwestern China, Aerosol. Air. Qual. Res, 19, 1007–1023,  
400 <https://doi.org/10.4209/aaqr.2018.11.0397>, 2019.
- Cristofanelli, P., Landi, T. C., Calzolari, F., Duchi, R., Marinoni, A., Rinaldi, M., and Bonasoni, P.: Summer atmospheric composition over  
the Mediterranean basin: Investigation on transport processes and pollutant export to the free troposphere by observations at the  
WMO/GAW Mt. Cimone global station (Italy, 2165 m a.s.l.), Atmos. Env., 141, 139–152, <https://doi.org/10.1016/j.atmosenv.2016.06.048>,  
2016.
- 405 Cui, Y., Lin, J., Song, C., Liu, M., Yan, Y., Xu, Y., and Huang, B.: Rapid growth in nitrogen dioxide pollution over Western China, 2005–  
2013, Atmos. Chem. Phys., 16, 6207–6221, <https://doi.org/10.5194/acp-16-6207-2016>, 2016.
- Davulienė, L., Jasineviciene, D., Garbariene, I., Andriejauskiene, J., Ulevicius, V., and Bycenkiene, S.: Long-term air pollution trend analysis  
in the South-eastern Baltic region, 1981–2017, Atmos. Res., 247, 105191, <https://doi.org/10.1016/j.atmosres.2020.105191>, 2021.

- 410 Deng, J. , Guo, H. , Zhang, H. , Zhu, J., Wang , X. and Fu, P.: Source apportionment of black carbon aerosols from light absorption observation and source-oriented modeling: an implication in a coastal city in China, *Atmos. Chem. Phys.*, 20, 14419–14435, <https://doi.org/10.5194/acp-20-14419-2020>, 2020.
- Duan, L., Yan, L., and Xiu, G.: Online Measurement of PM<sub>2.5</sub> at an Air Monitoring Supersite in Yangtze River Delta: Temporal Variation and Source Identification, *Atmosphere*, 11, 789, <https://doi.org/10.3390/atmos11080789>, 2020.
- 415 Fan, Q., Zhang, Y., Ma, W., Ma, H., Feng, J., Yu, Q., Yang, X., Ng, S. K. W., Fu, Q., and Chen, L.: Spatial and Seasonal Dynamics of Ship Emissions over the Yangtze River Delta and East China Sea and Their Potential Environmental Influence, *Env. Sci. Technol.*, 50, 1322–1329, <https://doi.org/10.1021/acs.est.5b03965>, 2016.
- Fang, G. W., Qingling , and Tian, L.: Green development of Yangtze River Delta in China under Population-Resources-Environment-Development-Satisfaction perspective, *Sci. Tot. Env.*, 727, <https://doi.org/10.1016/j.scitotenv.2020.138710>, 2020.
- 420 Gao, W., Tie, X., Xu, J., Huang, R., Mao, X., and Zhou, G. C., Luyu Long-term trend of O<sub>3</sub> in a mega City (Shanghai), China: Characteristics, causes, and interactions with precursors, *Sci. Tot. Env.*, 603–604, 425–433, <https://doi.org/10.1016/j.scitotenv.2017.06.099>, 2017.
- Hao, Y., and Song, X.: Research on trends and spatial distribution of vehicular emissions and its control measure assessment in the Yangtze River Delta, China, for 1999–2015, *Env. Sci. Pollut. R.*, 25, 36503–36517, <https://doi.org/10.1007/s11356-018-3476-y>, 2018.
- Kan, H., Chen, B., and Hong, C.: Health Impact of Outdoor Air Pollution in China: Current Knowledge and Future Research Needs, *Environ. Health Persp.*, 117, A187, <https://doi.org/10.1289/ehp.12737>, 2009.
- 425 Kan, H., Chen, R., and Tong, S.: Ambient air pollution, climate change, and population health in China, *Environ. Int.*, 42, 10–19, <https://doi.org/10.1016/j.envint.2011.03.003>, 2012.
- Kurokawa, J., and Ohara, T.: Long-term historical trends in air pollutant emissions in Asia: Regional Emission inventory in ASia (REAS) version 3, *Atmos. Chem. Phys.*, 20, 12761–12793, <https://doi.org/10.5194/acp-20-12761-2020>, 2020.
- 430 Li, L., Zhao, Q., Zhang, J., Li, H., Liu, Q., Li, C., Chen, F., Qiao, Y., and Han, J.: Bottom-up emission inventories of multiple air pollutants from open straw burning: A case study of Jiangsu province, Eastern China(Article), *Atmos. Pollut. Res.*, 10, 501–507, <https://doi.org/10.1016/j.apr.2018.09.011>, 2019.
- Li, M., Zhang, Q., Kurokawa, J. i., Woo, J.-H., He, K., Lu, Z., Ohara, T., Song, Y., Streets, D. G., Carmichael, G. R., Cheng, Y., Hong, C., Huo, H., Jiang, X., Kang, S., Liu, F., Su, H., and Zheng, B.: MIX: a mosaic Asian anthropogenic emission inventory under the international collaboration framework of the MICS-Asia and HTAP, *Atmos. Chem. Phys.*, 17, 935–963, <https://doi.org/10.5194/acp-17-935-2017>, 2017.
- 435 Li, M., Fang, W., Li, J., and Yang, F.: The overall variation characteristics of Akedala atmospheric background station of pollutants, *Env. Ecol.*, 1, 80–84, 2019.
- Li, R., Mei, X., Chen, L., Wang, L., Wang, Z., and Jing, Y.: Long-Term (2005–2017) View of Atmospheric Pollutants in Central China Using Multiple Satellite Observations, *Remote Sens-Basel*, 12, 1041, <https://doi.org/10.3390/rs12061041>, 2020.
- 440 Liang, D., Wang, Y.-q., Wang, Y.-j., and Ma, C.: National air pollution distribution in China and related geographic, gaseous pollutant, and socio-economic factors, *Env. Pollut.*, 250, 998–1009, <https://doi.org/10.1016/j.envpol.2019.03.075>, 2019.
- Lin, W., Xu, X., Yu, D., Dai, X., Zhang, Z., Meng, Z., and Wang, Y.: Quality Control for Reactive Gases Observation at Longfengshan Regional Atmospheric Background Monitoring Station, *Meteo. Mon.*, 35, 93–100, 2009.
- Lin, W., Xu, X., Sun, J., Li, Y., and Meng, Z.: Characteristics of gaseous pollutants at Jinsha, a remote mountain site in Central China, *Sci. China*, 41, 136–144, <https://doi.org/10.1360/032010-521>, 2011.

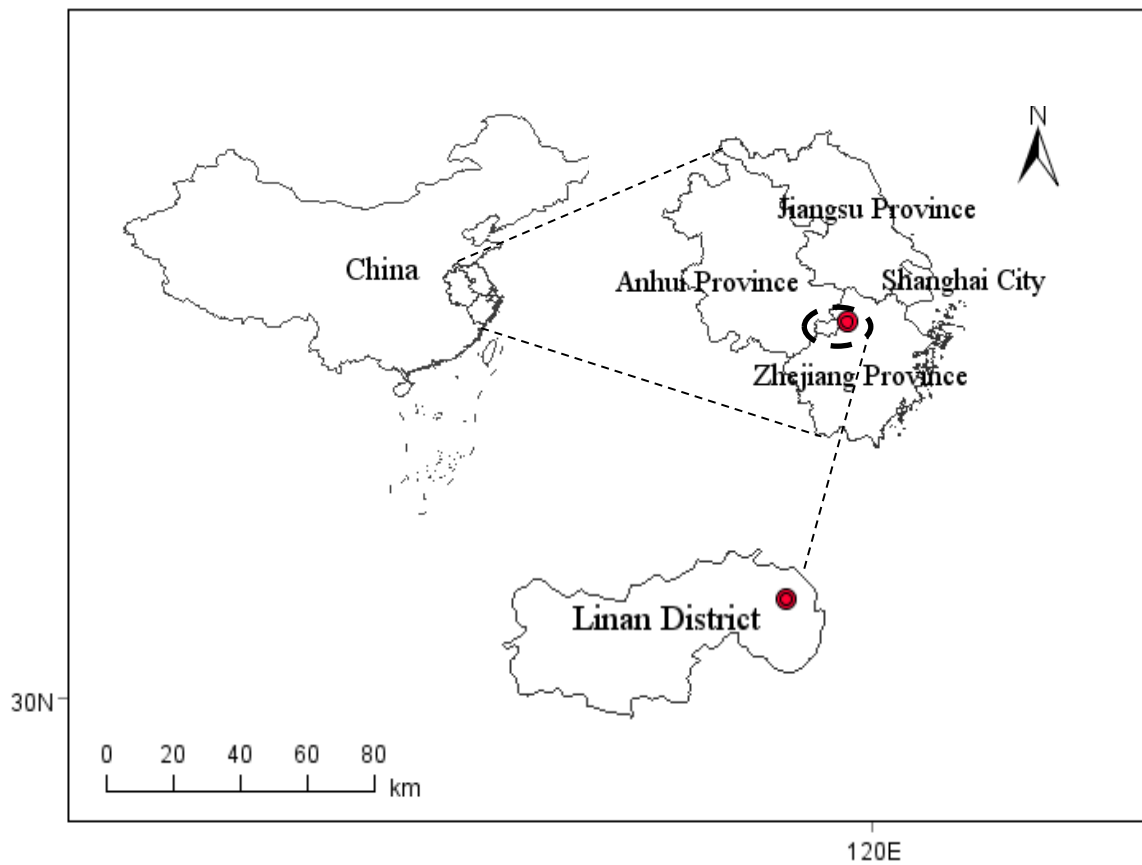
- 445 Lin, J. T., Martin, R. V., Boersma, K. F., Sneep, M., Stammes, P., Spurr, R., Wang, P., Van Roozendaal, M., Clémer, K. and Irie, H.: Retrieving tropospheric nitrogen dioxide from the Ozone Monitoring Instrument: Effects of aerosols, surface reflectance anisotropy, and vertical profile of nitrogen dioxide, *Atmos. Chem. Phys.*, 14, 1441–1461, <https://doi.org/10.5194/acp-14-1441-2014>, 2014.
- Lin, J. T., Liu, M. Y., Xin, J. Y., Boersma, K. F., Spurr, R., Martin, R., and Zhang, Q.: Influence of aerosols and surface reflectance on satellite NO<sub>2</sub> retrieval: seasonal and spatial characteristics and implications for NO<sub>x</sub> emission constraints, *Atmospheric Chemistry and*  
450 *Physics*, 15, 11217–11241, <https://doi.org/10.5194/acp-15-11217-2015>, 2015.
- Liu, M. Y., Lin, J. T., Boersma, K. F., Pinardi, G., Wang, Y., Chimot, J., Wagner, T., Xie, P., Eskes, H., Van Roozendaal, M., Hendrick, F., Wang, P., Wang, T., Yan, Y. Y., Chen, L. L., and Ni, R. J.: Improved aerosol correction for OMI tropospheric NO<sub>2</sub> retrieval over East Asia: constraint from CALIOP aerosol vertical profile, *Atmos. Meas. Techn.*, 12, 1–21, <https://doi.org/10.5194/amt-12-1-2019>, 2019.
- Lin, W., Ma, Z., Pu, W., Gao, W., Ma, Q., and Yu, D.: Quality Control Methods for Atmospheric Composition Observations - Reactive  
455 Gases, in *Meteorological industry standards in the People's Republic of China*, 2019.
- Liu, S., Jiang, X. T., Narcisse T. Lv, Chen, and Du, L.: Effects of NO<sub>x</sub>, SO<sub>2</sub> and RH on the SOA formation from cyclohexene photooxidation, *Chemosphere*, 216, 794–804, <https://doi.org/10.1016/j.chemosphere.2018.10.180>, 2019.
- Meng, Z. Y., Xu, X. B., Yan, P., Ding, G. A., Tang, J., Lin, W. L., Xu, X. D., and Wang, S. F.: Characteristics of trace gaseous pollutants at a regional background station in Northern China, *Atmos. Chem. Phys.*, 9, 927–936, <https://doi.org/10.5194/acp-9-927-2009>, 2009.
- 460 Mi, C., and Qin, X.: Annual Report on Motor Vehicle Pollution Prevention and Control in China (2010), *Yearbook of the People's Republic of China*, 0254–6108, 489, 2011.
- Pandey, S. K., Kim, K.-H., Chung, S. Y. C., S.J., Kim, M. Y., and Shon, Z. H.: Long-term study of NO<sub>x</sub> behavior at urban roadside and background locations in Seoul, Korea, *Atmos. Env.*, 42, 607–622, <https://doi.org/10.1016/j.atmosenv.2007.10.015>, 2008.
- Qi, H., Lin, W., Xu, X., Yu, X., and Ma, Q.: Significant downward trend of SO<sub>2</sub> observed from 2005 to 2010 at a background station in the  
465 Yangtze Delta region, China, *Science China Chemistry* 55, 1451–1458, <https://doi.org/10.1007/s11426-012-4524-y>, 2012.
- Resmi, C., Nishanth, T., Satheesh Kumar, M., Balachandramohan, M., and Valsaraj, K.: Long-Term Variations of Air Quality Influenced by Surface Ozone in a Coastal Site in India: Association with Synoptic Meteorological Conditions with Model Simulations, *Atmosphere*, 11, 193, <https://doi.org/10.3390/atmos11020193>, 2020.
- Shen, J., He, L., Chen, P., Xie, M., Jiang, M., Chen, D., and Zhou, G.: Characteristics of Ozone Concentration Variation in the Northern  
470 Background Site of the Pearl River Delta, *Eco. Environ. Sci.*, 28, 2006–2011, <https://doi.org/10.16258/j.cnki.1674-5906.2019.10.010>, 2019.
- Shi, Y., Zhu, S., Li, L., Chen, Y., An, J., and Fu, Z.: Historical trends and spatial distributions of major air pollutants in the Yangtze River Delta, *J. Lanzhou Univ. (Natural Sci.)*, 54, 184–191, 199, <https://doi.org/10.13885/j.issn.0455-2059.2018.02.007>, 2018.
- Squizzato, S., Masiol, M., Rich, D. Q., and Hopke, P. K.: PM<sub>2.5</sub> and gaseous pollutants in New York State during 2005–2016: spatial  
475 variability, temporal trends, and economic influences, *Atmos. Env.*, 183, 209–224, <https://doi.org/10.1016/j.atmosenv.2018.03.045>, 2018.
- Su, B., Liu, X., and Tao, J.: Background characteristics of SO<sub>2</sub>, NO<sub>x</sub> and CO in forest and alpine background areas of eastern China, *Environ. Monit. China* 15–21, 2013.
- Sun, W., Shao, M., Granier, C., Liu, Y., Ye, C., and Zheng, J.: Long-Term Trends of Anthropogenic SO<sub>2</sub>, NO<sub>x</sub>, CO, and NMVOCs Emissions in China (Article), *Earth's Future*, 6, 1112–1133, <https://doi.org/10.1029/2018ef000822>, 2018.

- 480 Swartz, J. S., Van Zyl, P. G., Beukes, J. P., Labuschagne, C. B., E. G. , Portafaix, T., Galy-Lacaux, C., and Pienaar, J. J.: Twenty-one years of passive sampling monitoring of SO<sub>2</sub>, NO<sub>2</sub> and O<sub>3</sub> at the Cape Point GAW station, South Africa, *Atmos. Environ.*, 222, <https://doi.org/10.1016/j.atmosenv.2019.117128>, 2020a.
- Swartz, J. S., Zyl, P. G. v., Beukes, J. P., Galy-Lacaux, C., Ramandh, A., and Pienaar, J. J.: Measurement report: Statistical modelling of long-term trends of atmospheric inorganic gaseous species within proximity of the pollution hotspot in South Africa, *Atmos. Chem. Phys.*, 20, 10637–10665, <https://doi.org/10.5194/acp-20-10637-2020>, 2020b.
- 485 US EPA: Quality Assurance Handbook for Air Pollution Measurement Systems, Volume II, Ambient Air Quality Monitoring Program, EPA-454/B-17-001, 2017.
- Wan, Z., Ji, S., Liu, Y., Zhang, Q., Chen, J., and Wang, Q.: Shipping emission inventories in China's Bohai Bay, Yangtze River Delta, and Pearl River Delta in 2018(Article), *Mar. Pollution. Bulletin.*, 151, <https://doi.org/10.1016/j.marpolbul.2019.110882>, 2020.
- 490 Wang, H. L., Qiao, L. P., Lou, S. R., Zhou, M., Ding, A. J., Huang, H. Y., Chen, J. M., Wang, Q., Tao, S. K., Chen, C. H., Li, L., and Huang, C.: Chemical composition of PM<sub>2.5</sub> and meteorological impact among three years in urban Shanghai, China, *J. Clean. Prod.*, 112, 1302–1311, <https://doi.org/10.1016/j.jclepro.2015.04.099>, 2016.
- Wang, L. Yuan, L, Zhang, X. L. , Jia, Y. T. : Characteristics and Source Apportionment of Black Carbon in Chengdu, *Environ. Sci.*, 41 , 0250–3301, <https://doi.org/10.13227/j.hjcx.201908190>, 2020.
- 495 Wang, N., Lyu, X., Deng, X., Huang, X., Jiang, F., and Ding, A.: Aggravating O<sub>3</sub> pollution due to NO<sub>x</sub> emission control in eastern China, *Sci. Total. Environ.*, 677, 732–744, <https://doi.org/10.1016/j.scitotenv.2019.04.388>, 2019.
- Wang, T., He, H., Xia, Z., Wu, M., and Zhang, Q.: Pollution characteristics of SO<sub>2</sub>, NO<sub>2</sub>, CO and O<sub>3</sub> in Nanjing in 2015, *Chinese J. Environ. Engi.*, 11, 4155–4161, 2017.
- Wang, Y. Q.: MeteoInfo: GIS software for meteorological data visualization and analysis, *Meteorol. Appl.*, 21, 360–368, 2014.
- 500 <https://doi.org/10.1002/met.13>
- Xie, Z.: Global Financial Crisis Making a V-Shaped Fluctuation in NO<sub>2</sub> Pollution over the Yangtze River Delta, *J. Meteorol. Res-Prc*, 31, 438–447, <https://doi.org/10.1007/s13351-017-6053-2>, 2017b.
- Xin, Y. J., Wang, G. C., and Chen, L.: Identification of Long-Range Transport Pathways and Potential Sources of PM<sub>10</sub> in Tibetan Plateau Uplift Area: Case Study of Xining, China in 2014, *Aerosol. Air. Qual. Res.*, 16, 1044–1054, <https://doi.org/10.4209/aaqr.2015.05.0296>,
- 505 2016. Xu, X., Lin, W., Yan, P., Zhang, Z., and Yu, X.: Long-term Changes of Acidic Gases in China's Yangtze Delta and Northeast Plain Regions During 1994–2006, *Adv. Clim. Change. Res.*, 195–201, 2008.
- Xu, X., Yang, B., Shi, S., Wang, X., and He, H.: Analysis on the Current Situation of Acid Rain Pollution in Lin'an District of Hangzhou City, *J. Anhui. Agricul. sci.*, 47, 86–89, 92, <https://doi.org/10.3969/j.issn.0517-6611.2019.09.025>, 2019.
- Xue, R., Wang, S. L., Danran , Zou, Z., Chan, K. L., Valks, P., Saiz-Lopez, Alfonso, and Zhou, B.: Spatio-temporal variations in NO<sub>2</sub> and SO<sub>2</sub> over Shanghai and Chongming Eco-Island measured by Ozone Monitoring Instrument (OMI) during 2008–2017, *J. Clean. Prod.*, 258, <https://doi.org/10.1016/j.jclepro.2020.120563>, 2020.
- 510 Yan, F., Chen, W., Jia, S., Zhong, B., Yang, L., Mao, J., Chang, M., Shao, M., Yuan, B., Situ, S., Wang, X., and Wang, D. C. X.: Stabilization for the secondary species contribution to PM<sub>2.5</sub> in the Pearl River Delta (PRD) over the past decade, China: A meta-analysis, *Atoms. Env.*, 242, 117817, <https://doi.org/10.1016/j.atmosenv.2020.117817>, 2020.
- 515 Yang, B., and Luo, R.: Research progress of air pollution in Yangtze River Delta, *Environ. Ecol.*, 1, 74–78, 2019.

- Yang, J., Xin, J., Ji, D., and Zhu, B.: Variation Analysis of Background Atmospheric Pollutants in North China During the Summer of 2008 to 2011, *Environ. Sci.*, 3693–3704, 2012.
- Yang, Q.: Characteristics and Causes of Acid Rain Changes in Xiaoshan District, 2008–2017, *Overs. Dig.*, 2018.
- 520 Yu, Y., Wang, Z., Cui, X., Chen, F., and Xu, H.: Effects of Emission Reductions of Key Sources on the PM<sub>2.5</sub> Concentrations in the Yangtze River Delta, *Environ. Sci.*, 40, 11–23, <https://doi.org/10.13227/j.hjx.201804105>, 2019.
- Zhao, B., Wang, S., Wang, J., Fu, J. S., Liu, T., Xu, J., Fu, X., and Hao, J.: Impact of national NO<sub>x</sub> and SO<sub>2</sub> control policies on particulate matter pollution in China, *Atmos. Env.*, 77, 453–463, <https://doi.org/10.1016/j.atmosenv.2013.05.012>, 2013.
- Zhao, M., Qiao, T., Huang, Z., Zhu, M., Xu, W., Xiu, G., Tao, J., and Lee, S.: Comparison of ionic and carbonaceous compositions of PM<sub>2.5</sub> in 2009 and 2012 in Shanghai, China, *Sci. Tot. Env.*, 536, 695–703, [doi.org/10.1016/j.scitotenv.2015.07.100](https://doi.org/10.1016/j.scitotenv.2015.07.100), 2015.
- 525 Zhao, P., Tuygun, G. T., Li, B., Liu, J., Yuan, L., Luo, Y., Xiao, H., and Zhou, Y.: The effect of environmental regulations on air quality: A long-term trend analysis of SO<sub>2</sub> and NO<sub>2</sub> in the largest urban agglomeration in Southwest China, *Atmos. Pollut. Res.*, <https://doi.org/10.1016/j.apr.2019.09.011>, 2019.
- Zhao, S., Liu, S., Hou, X., Cheng, F., Wu, X., Dong, S., and Beazley, R.: Temporal dynamics of SO<sub>2</sub> and NO<sub>x</sub> pollution and contributions of driving forces in urban areas in China, *Environ. Pollut.*, 242, 239–248, <https://doi.org/10.1016/j.envpol.2018.06.085>, 2018.
- 530 Zheng, S., Yi, H., and Li, H.: The impacts of provincial energy and environmental policies on air pollution control in China, *Renew. Sust. Energ. Rev.*, 49, 386–394, <https://doi.org/10.1016/j.rser.2015.04.088>, 2015.
- Zhou, D., Tian, X., Cai, Z., Wang, X., Li, Y., Liu, Y., and Jiang, F.: Evaluation of Ozone Change and Control Effects in Yangtze River Delta Region During G20 Summit, *Environ. Monit. in China*, 36, 41–49, <https://doi.org/10.19316/j.issn.1002-6002.2020.02.06>, 2020.
- Department of Ecology and Environment of Zhejiang Province , Bulletin on the ecological environment of Zhejiang Province in 2006, 535 [http://sthjt.zj.gov.cn/art/2007/6/5/art\\_1201912\\_13471624.html](http://sthjt.zj.gov.cn/art/2007/6/5/art_1201912_13471624.html), last access: 24 June 2021.
- Department of Ecology and Environment of Zhejiang Province , Bulletin on the ecological environment of Zhejiang Province in 2007, [http://sthjt.zj.gov.cn/art/2008/6/5/art\\_1201912\\_13471634.html](http://sthjt.zj.gov.cn/art/2008/6/5/art_1201912_13471634.html), last access: 24 June 2021.
- Department of Ecology and Environment of Zhejiang Province , Bulletin on the ecological environment of Zhejiang Province in 2008, [http://sthjt.zj.gov.cn/art/2009/6/5/art\\_1201912\\_13471647.html](http://sthjt.zj.gov.cn/art/2009/6/5/art_1201912_13471647.html), last access: 24 June 2021.
- 540 Department of Ecology and Environment of Zhejiang Province , Bulletin on the ecological environment of Zhejiang Province in 2009, [http://sthjt.zj.gov.cn/art/2010/6/5/art\\_1201912\\_13471671.html](http://sthjt.zj.gov.cn/art/2010/6/5/art_1201912_13471671.html), last access: 24 June 2021.
- Department of Ecology and Environment of Zhejiang Province , Bulletin on the ecological environment of Zhejiang Province in 2010, [http://sthjt.zj.gov.cn/art/2011/6/3/art\\_1201912\\_13471687.html](http://sthjt.zj.gov.cn/art/2011/6/3/art_1201912_13471687.html), last access: 24 June 2021.
- Department of Ecology and Environment of Zhejiang Province , Bulletin on the ecological environment of Zhejiang Province in 2011, 545 [http://sthjt.zj.gov.cn/art/2012/6/4/art\\_1201912\\_15028444.html](http://sthjt.zj.gov.cn/art/2012/6/4/art_1201912_15028444.html), last access: 24 June 2021.
- Department of Ecology and Environment of Zhejiang Province , Bulletin on the ecological environment of Zhejiang Province in 2012, [http://sthjt.zj.gov.cn/art/2013/6/5/art\\_1201912\\_15028442.html](http://sthjt.zj.gov.cn/art/2013/6/5/art_1201912_15028442.html), last access: 24 June 2021.
- Department of Ecology and Environment of Zhejiang Province , Bulletin on the ecological environment of Zhejiang Province in 2013, [http://sthjt.zj.gov.cn/art/2014/6/4/art\\_1201912\\_13471699.html](http://sthjt.zj.gov.cn/art/2014/6/4/art_1201912_13471699.html), last access: 24 June 2021.
- 550 Department of Ecology and Environment of Zhejiang Province , Bulletin on the ecological environment of Zhejiang Province in 2014, [http://sthjt.zj.gov.cn/art/2015/6/3/art\\_1201912\\_13471712.html](http://sthjt.zj.gov.cn/art/2015/6/3/art_1201912_13471712.html), last access: 24 June 2021.

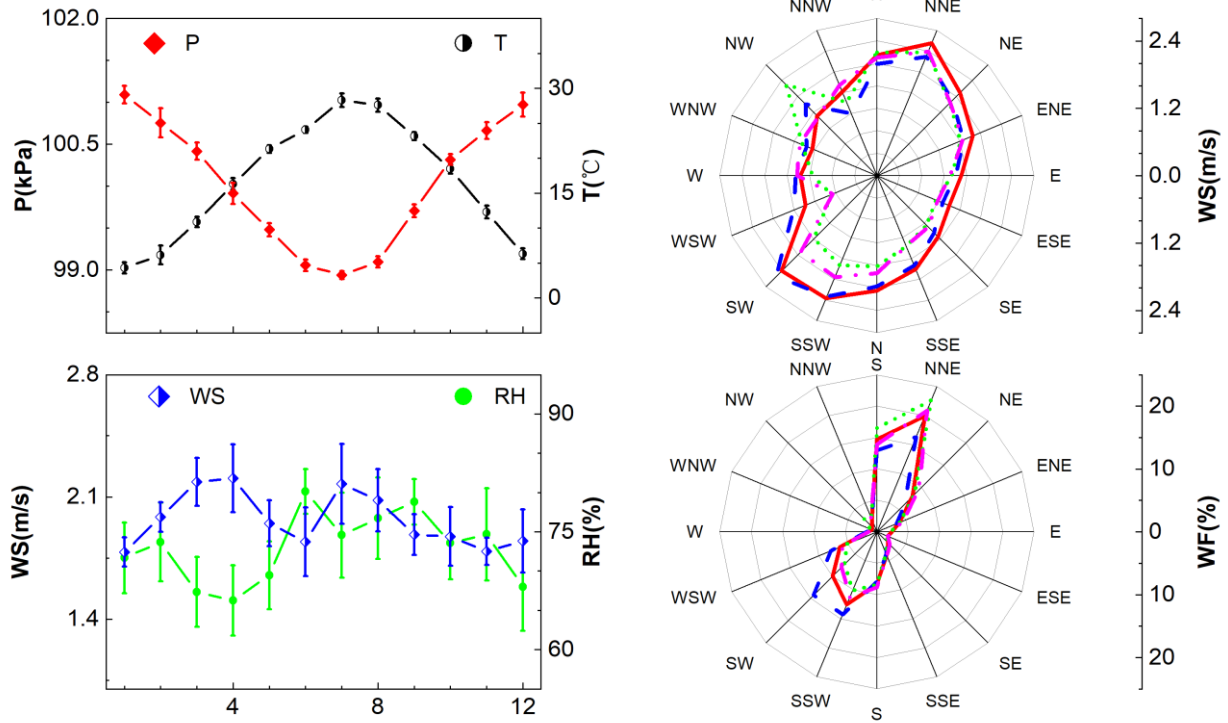
- Department of Ecology and Environment of Zhejiang Province , Bulletin on the ecological environment of Zhejiang Province in 2015, [http://sthjt.zj.gov.cn/art/2016/6/2/art\\_1201912\\_13471725.html](http://sthjt.zj.gov.cn/art/2016/6/2/art_1201912_13471725.html), last access: 24 June 2021.
- Department of Ecology and Environment of Zhejiang Province , Bulletin on the ecological environment of Zhejiang Province in 2016, 555 [http://sthjt.zj.gov.cn/art/2017/6/2/art\\_1201912\\_13471748.html](http://sthjt.zj.gov.cn/art/2017/6/2/art_1201912_13471748.html), last access: 24 June 2021.
- Department of Ecology and Environment of Jiangsu Province, Bulletin on the ecological environment of Jiangsu Province in 2006, [http://hbt.jiangsu.gov.cn/art/2007/3/28/art\\_1649\\_3939925.html](http://hbt.jiangsu.gov.cn/art/2007/3/28/art_1649_3939925.html), last access: 24 June 2021.
- Department of Ecology and Environment of Jiangsu Province, Bulletin on the ecological environment of Jiangsu Province in 2007, [http://hbt.jiangsu.gov.cn/art/2008/3/28/art\\_1649\\_3939926.html](http://hbt.jiangsu.gov.cn/art/2008/3/28/art_1649_3939926.html), last access: 24 June 2021.
- 560 Department of Ecology and Environment of Jiangsu Province, Bulletin on the ecological environment of Jiangsu Province in 2008, [http://hbt.jiangsu.gov.cn/art/2009/6/5/art\\_1649\\_3939927.html](http://hbt.jiangsu.gov.cn/art/2009/6/5/art_1649_3939927.html), last access: 24 June 2021.
- Department of Ecology and Environment of Jiangsu Province, Bulletin on the ecological environment of Jiangsu Province in 2009, [http://hbt.jiangsu.gov.cn/art/2010/6/22/art\\_1649\\_3939928.html](http://hbt.jiangsu.gov.cn/art/2010/6/22/art_1649_3939928.html), last access: 24 June 2021.
- Department of Ecology and Environment of Jiangsu Province, Bulletin on the ecological environment of Jiangsu Province in 2010, 565 [http://hbt.jiangsu.gov.cn:8080/art/2011/6/2/art\\_1677\\_4232467.html](http://hbt.jiangsu.gov.cn:8080/art/2011/6/2/art_1677_4232467.html), last access: 24 June 2021.
- Department of Ecology and Environment of Jiangsu Province, Bulletin on the ecological environment of Jiangsu Province in 2011, [http://www.jiangsu.gov.cn/art/2012/5/30/art\\_46750\\_2680095.html](http://www.jiangsu.gov.cn/art/2012/5/30/art_46750_2680095.html), last access: 24 June 2021.
- Department of Ecology and Environment of Jiangsu Province, Bulletin on the ecological environment of Jiangsu Province in 2012, [http://hbt.jiangsu.gov.cn/art/2013/6/5/art\\_1649\\_3939931.html](http://hbt.jiangsu.gov.cn/art/2013/6/5/art_1649_3939931.html), last access: 24 June 2021.
- 570 Department of Ecology and Environment of Jiangsu Province, Bulletin on the ecological environment of Jiangsu Province in 2013, <https://news.bjx.com.cn/html/20140604/515937.shtml>, last access: 24 June 2021.
- Department of Ecology and Environment of Jiangsu Province, Bulletin on the ecological environment of Jiangsu Province in 2014, <https://huanbao.bjx.com.cn/news/20150604/626623.shtml>, last access: 24 June 2021.
- Department of Ecology and Environment of Jiangsu Province, Bulletin on the ecological environment of Jiangsu Province in 2015, 575 [http://www.jiangsu.gov.cn/art/2016/6/24/art\\_46580\\_2555980.html](http://www.jiangsu.gov.cn/art/2016/6/24/art_46580_2555980.html), last access: 24 June 2021.
- Department of Ecology and Environment of Jiangsu Province, Bulletin on the ecological environment of Jiangsu Province in 2016, [http://hbt.jiangsu.gov.cn/art/2017/4/15/art\\_1649\\_3939935.html](http://hbt.jiangsu.gov.cn/art/2017/4/15/art_1649_3939935.html), last access: 24 June 2021.
- Department of Ecology and Environment of Shanghai city, Bulletin on the ecological environment of Shanghai city in 2006, <https://link.sthj.sh.gov.cn/file/2006bulletin/contents.htm>, last access: 24 June 2021.
- 580 Department of Ecology and Environment of Shanghai city, Bulletin on the ecological environment of Shanghai city in 2007, <https://link.sthj.sh.gov.cn/file/2007bulletin/index.htm> , last access: 24 June 2021.
- Department of Ecology and Environment of Shanghai city, Bulletin on the ecological environment of Shanghai city in 2008, <https://link.sthj.sh.gov.cn/file/2008bulletin/index.html>, last access: 24 June 2021.
- Department of Ecology and Environment of Shanghai city, Bulletin on the ecological environment of Shanghai city in 2009, 585 <https://link.sthj.sh.gov.cn/file/2009bulletin/index.html> , last access: 24 June 2021.
- Department of Ecology and Environment of Shanghai city, Bulletin on the ecological environment of Shanghai city in 2010, <https://link.sthj.sh.gov.cn/file/2010bulletin/ch/cont.html> , last access: 24 June 2021.

- Department of Ecology and Environment of Shanghai city, Bulletin on the ecological environment of Shanghai city in 2011, <https://link.sthj.sh.gov.cn/file/2011bulletin/index.html>, last access: 24 June 2021.
- 590 Department of Ecology and Environment of Shanghai city, Bulletin on the ecological environment of Shanghai city in 2013, <https://link.sthj.sh.gov.cn/file/2014bulletin/index.html>, last access: 24 June 2021.
- Department of Ecology and Environment of Shanghai city, Bulletin on the ecological environment of Shanghai city in 2014, <https://sthj.sh.gov.cn/assets/html/117972-02.pdf>, last access: 24 June 2021.
- Department of Ecology and Environment of Shanghai city, Bulletin on the ecological environment of Shanghai city in 2015, <https://sthj.sh.gov.cn/hbzhywpt1143/hbzhywpt1144/20160329/0024-141845.html>, last access: 24 June 2021.
- 595 Department of Ecology and Environment of Shanghai city, Bulletin on the ecological environment of Shanghai city in 2016, <https://sthj.sh.gov.cn/hbzhywpt1143/hbzhywpt1144/20170601/0024-141846.html>, last access: 24 June 2021.

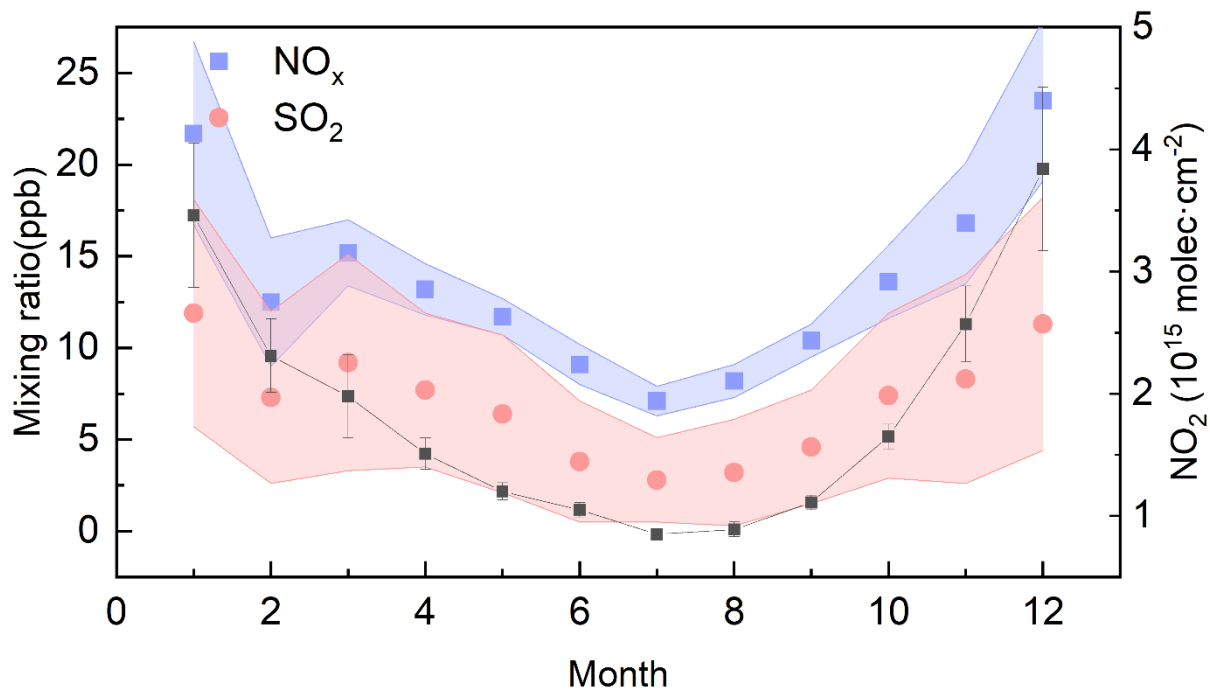


600

**Figure 1: Geographical location of LAN.**



605 **Figure 2: Average seasonal variations in air pressure (P), temperature (T), wind speed (WS), relative humidity (RH), and rose maps of wind speed (WS) and wind direction frequency (WF) at LAN during 2006–2016. In the rose maps of WS and WF, red solid represents spring, blue dash for summer, green short dot for autumn and magenta dash dot for winter.**



610 **Figure 3: Monthly average NO<sub>x</sub> and SO<sub>2</sub> mixing ratios at LAN (left axis) and monthly tropospheric vertical column density of NO<sub>2</sub> (right axis) over 115.125° E–122.875° E and 27.125° N–35.875° N in the YRD during 2006–2016.**

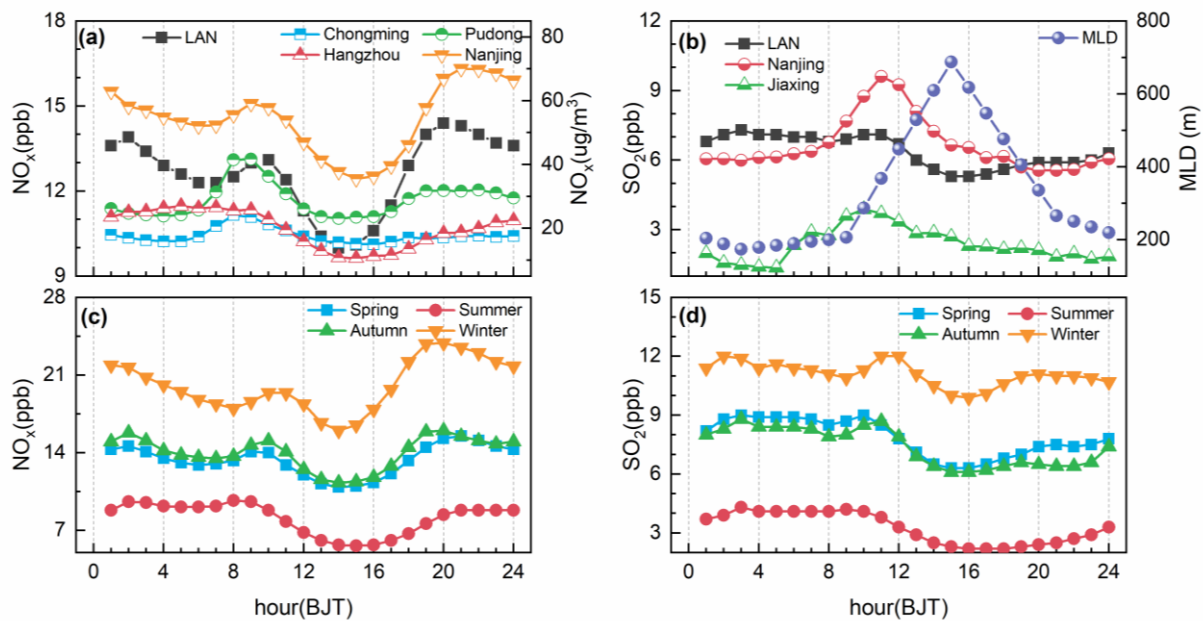
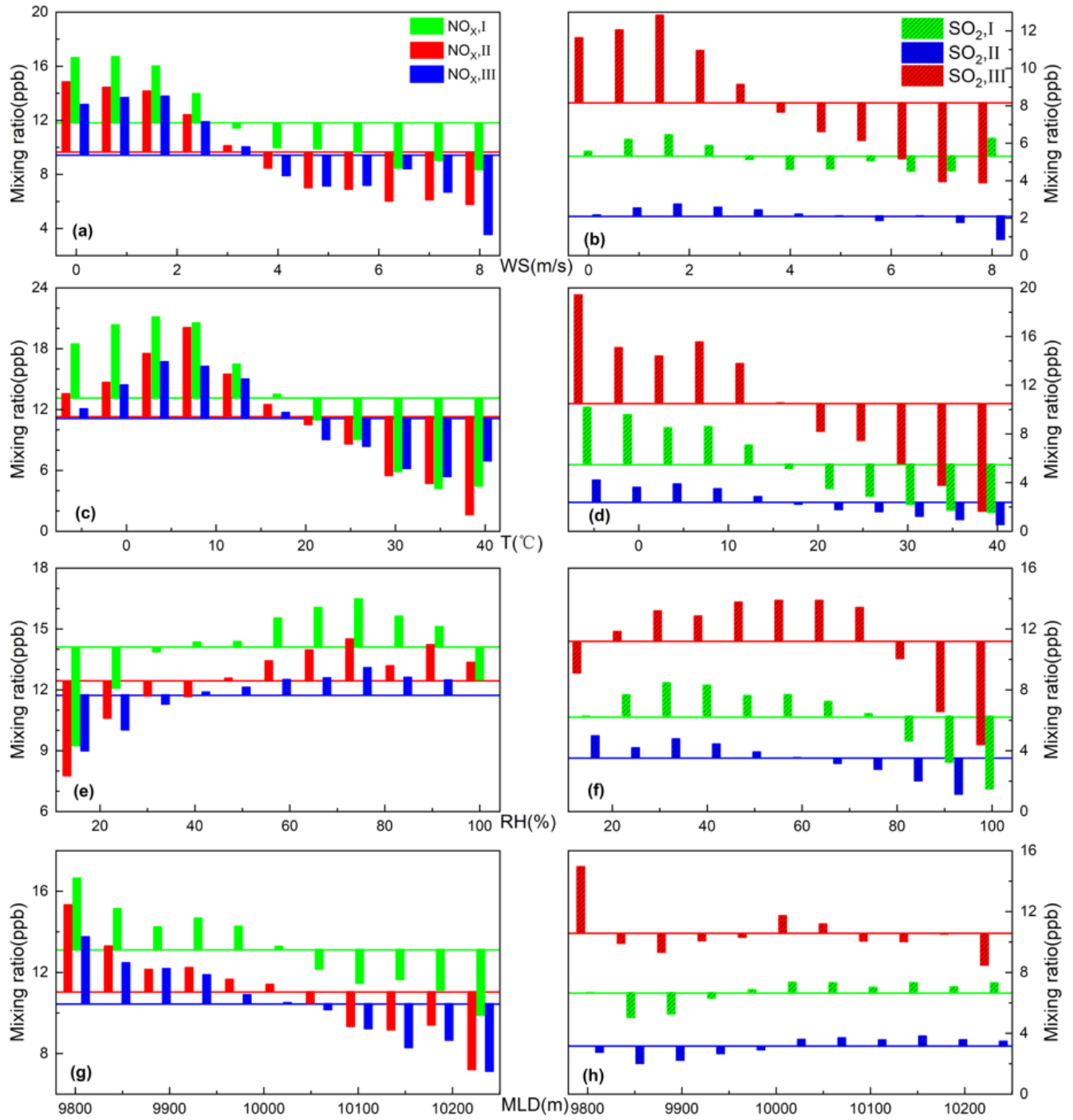
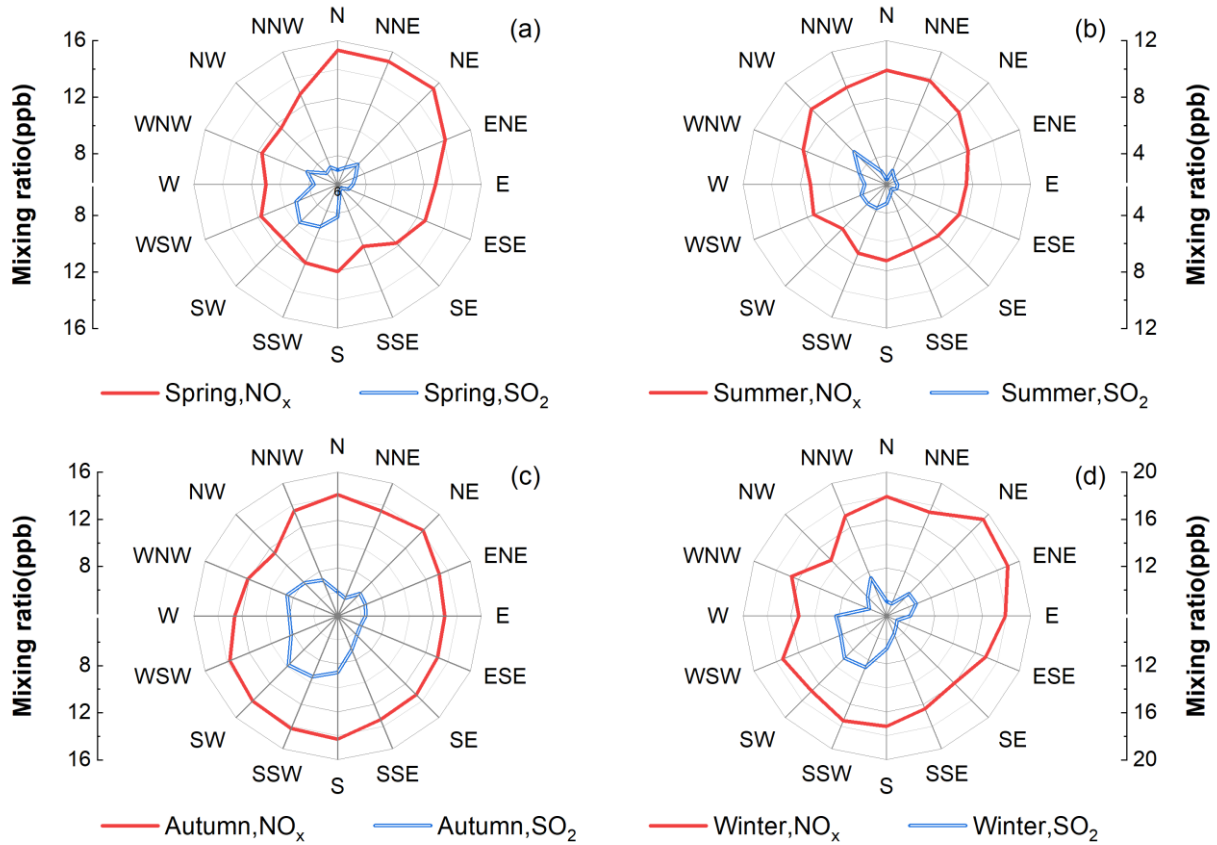


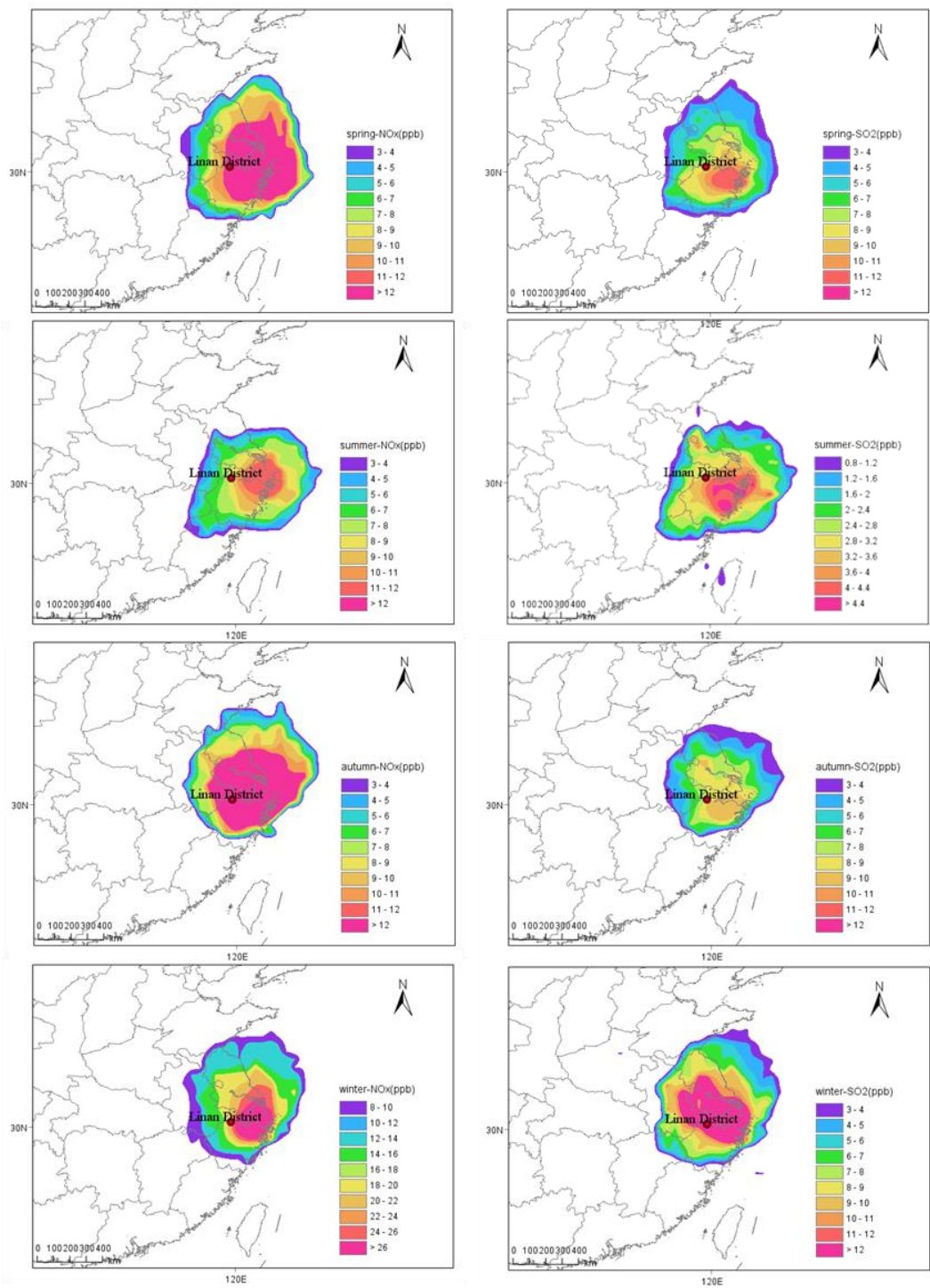
Figure 4: Annual average diurnal variations in NO<sub>x</sub> (a, left axis) and in SO<sub>2</sub> (b, left axis) at LAN and its surrounding cities (NO<sub>x</sub>, a, right axis; SO<sub>2</sub>, b, left axis); seasonal average diurnal variations in NO<sub>x</sub> (c, left axis) and SO<sub>2</sub> (d, left axis) at LAN. The average diurnal mixed layer depth (MLD; right axis) is also plotted in panel b.



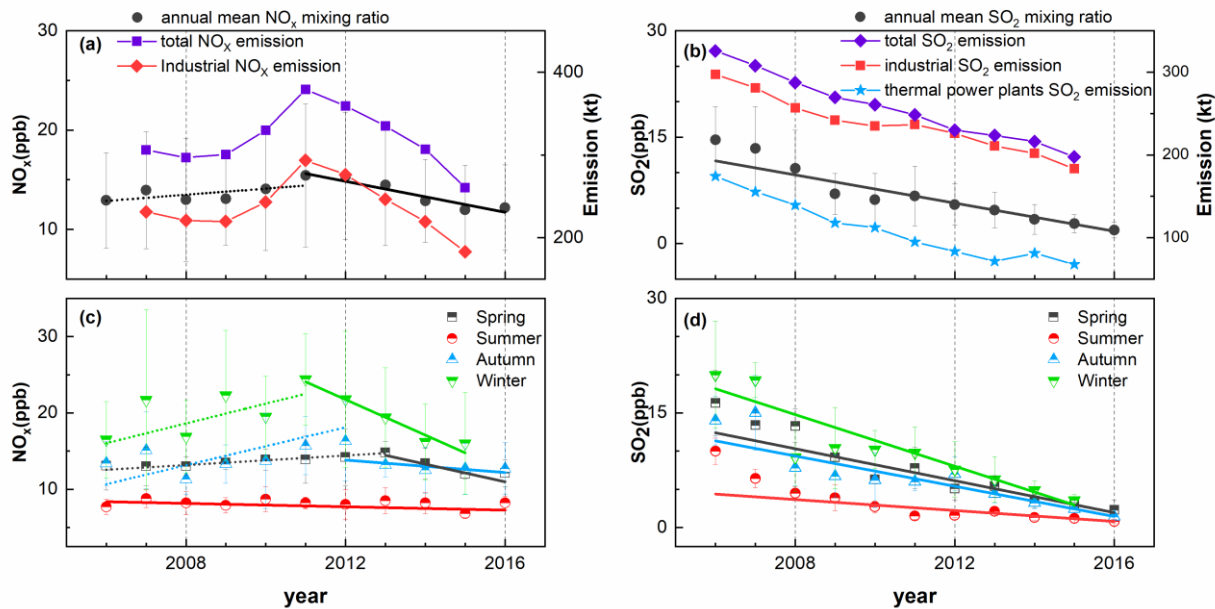
**Figure 5:** Variation characteristics of  $\text{NO}_x$  and  $\text{SO}_2$  with wind speed (WS; a and b), temperature (T; c and d), relative humidity (RH; e and f), and the mixed layer depth (MLD; g and h) at LAN during period I (2006–2009), period II (2010–2013) and period III (2014–2016). The horizontal lines in the graph indicate the average values of  $\text{NO}_x$  and  $\text{SO}_2$  for each period. Columns indicate changes relative to the corresponding mean values.



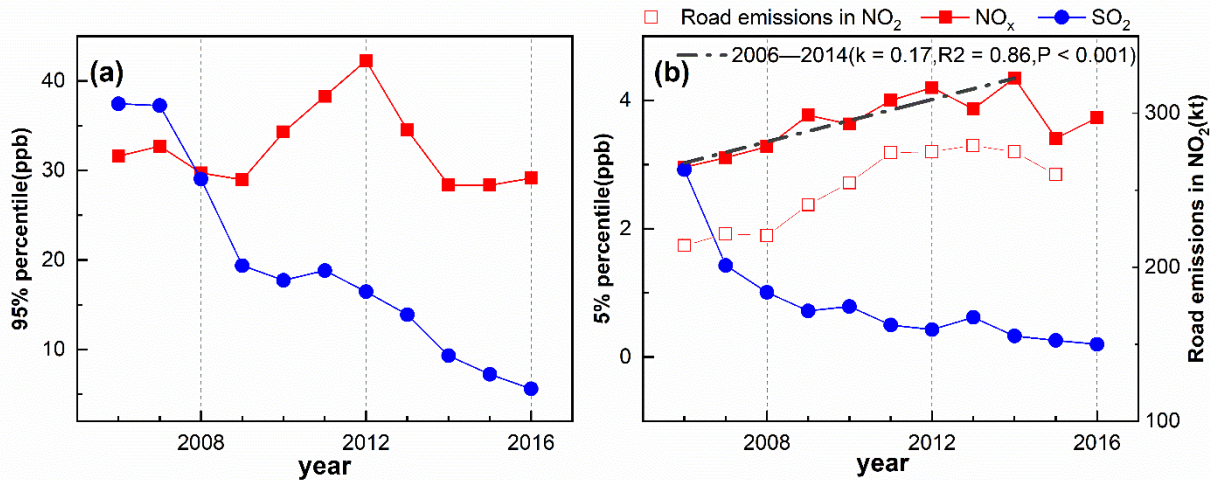
**Figure 6:** Seasonal distributions of  $\text{NO}_x$  and  $\text{SO}_2$  concentrations in different wind directions.



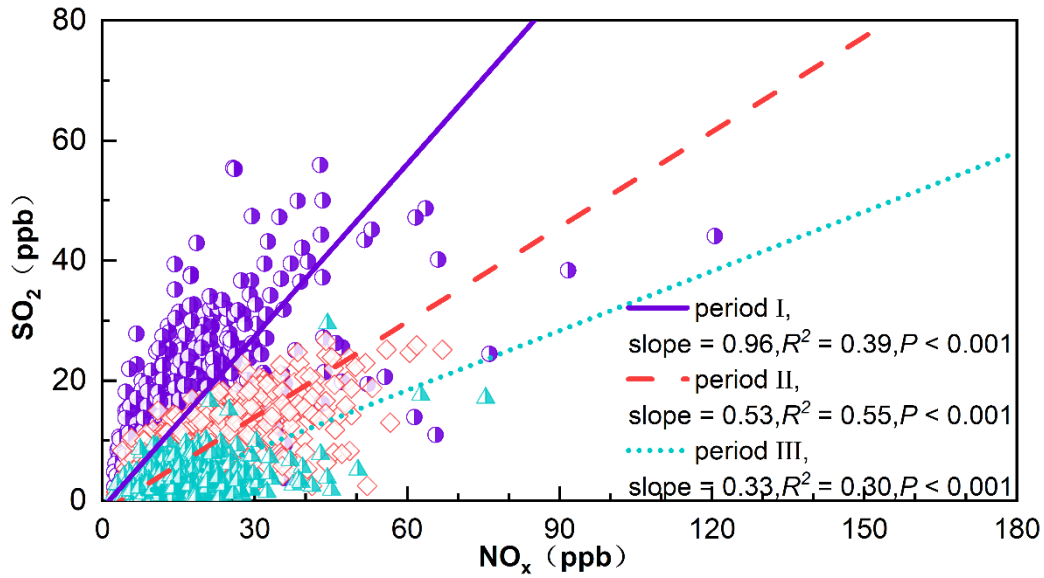
625 **Figure 7: Potential source analysis of NO<sub>x</sub> and SO<sub>2</sub> in different seasons at LAN according to concentration weighted trajectory analysis.**



630 **Figure 8:** Annual mean NO<sub>x</sub> mixing ratio at LAN (left axis) compared with total NO<sub>x</sub> emission and industrial NO<sub>x</sub> emission in the YRD (a, right axis); annual mean SO<sub>2</sub> mixing ratio at LAN (left axis) compared with total SO<sub>2</sub> emission, industrial SO<sub>2</sub> emission, thermal power plants SO<sub>2</sub> emission in the YRD (b, right axis), seasonal average annual variation of NO<sub>x</sub> (c), and SO<sub>2</sub> (d) at LAN.



635 **Figure 9:** Annual variations in the 95 % percentile concentration (a) and the 5 % percentile concentration (b) of NO<sub>x</sub> and SO<sub>2</sub> at LAN; data of NO<sub>2</sub> road emissions in the YRD are obtained from the REASv3.2 data sets in the *Regional Emission inventory in Asia* (Kurokawa and Ohara, 2020).



640 **Figure 10:** Reduced major axis regressions on the scatter plots of daily average SO<sub>2</sub> and NO<sub>x</sub> mixing ratios during three periods at LAN.

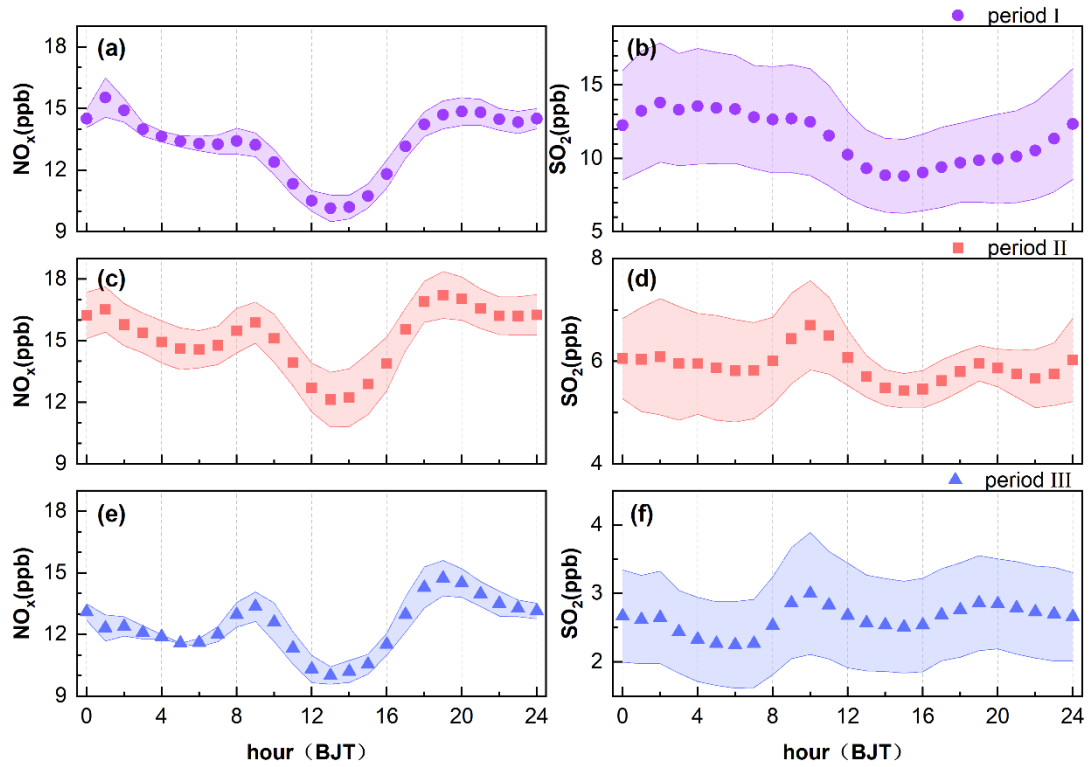


Figure 11: Average diurnal variations in NO<sub>x</sub> (a, c, e) and in SO<sub>2</sub> (b, d, f) during period I (2006–2009), period II (2010–2013) and period III (2014–2016) at LAN.

Table 1 Statistics of NO<sub>x</sub> and SO<sub>2</sub> levels from 2006 to 2016 at LAN.

year	NO <sub>2</sub> (ppb)					NO <sub>x</sub> (ppb)					SO <sub>2</sub> (ppb)					SO <sub>2</sub> /NO <sub>x</sub>
	Ave	Med	SD	Max	Min	Ave	Med	SD	Max	Min	Ave	Med	SD	Max	Min	
<b>2006</b>	12.1	10.9	4.2	19.9	6.0	12.9	11.5	4.8	22.0	6.5	14.6	13.8	4.7	24.7	8.4	1.13
<b>2007</b>	12.7	11.3	5.1	24.9	6.8	13.8	11.7	6.0	29.0	7.5	13.4	12.4	5.9	23.4	5.2	0.97
<b>2008</b>	12.0	10.8	5.0	22.5	6.2	13.0	11.3	6.2	27.9	6.6	10.6	10.6	5.4	19.9	3.7	0.82
<b>2009</b>	12.1	13.1	3.7	20.1	6.7	13.1	13.8	4.7	24.9	7.0	7.0	7.1	2.9	11.9	2.1	0.54
<b>2010</b>	12.5	11.6	5.1	24.5	6.5	14.1	12.5	6.2	29.3	7.6	6.2	5.7	3.7	14.9	1.9	0.44
<b>2011</b>	14.1	13.0	6.0	26.5	6.7	15.4	13.8	7.2	31.3	7.5	6.7	6.7	4.2	13.7	1.1	0.44
<b>2012</b>	13.8	14.8	5.4	22.2	5.6	15.4	15.8	6.4	26.8	5.9	5.5	6.0	2.9	9.3	1.3	0.36
<b>2013</b>	13.5	12.5	5.4	23.8	6.2	14.5	13.1	6.1	27.0	6.5	4.7	4.3	2.5	10.0	1.9	0.32
<b>2014</b>	12.1	11.8	3.7	18.8	7.0	12.9	12.4	4.2	20.2	7.3	3.4	3.0	2.1	8.6	1.0	0.26
<b>2015</b>	11.0	11.3	3.7	17.4	6.1	12.0	11.7	4.5	19.9	6.4	2.8	2.9	1.3	5.7	1.1	0.23
<b>2016</b>	11.1	10.7	3.4	16.8	6.8	12.2	11.4	4.3	19.8	7.2	1.9	1.6	1.1	3.7	0.6	0.16
<b>Ave.</b>	12.5	12.0	4.6	21.6	6.4	13.6	13.1	1.2	15.4	12.0	7.0	6.2	4.2	14.6	1.9	0.52

Ave: Average; Med: Median; SD: standard deviation; Max: maximum; Min: minimum.

**Table 2 NO<sub>x</sub> and SO<sub>2</sub> mixing ratios observed at various atmospheric background stations.**

Station	Latitude and longitude, altitude	Period of observation	NO <sub>x</sub> /ppb	SO <sub>2</sub> /ppb	SO <sub>2</sub> /NO <sub>x</sub>	References
Lin'an*, Yangtze River Delta background station	30.3° N, 119.73° E, 138 m a.s.l.	2006.1–2016.12	13.6 ± 1.2	7.0 ± 4.2	0.55	This study
Shangdianzi*, North China Regional Background Station	40.39° N, 117.07° E, 293.9 m a.s.l	2006.1–2006.12	12.7 ± 11.8	7.6 ± 10.2	0.60	(Meng et al., 2009)
Wuyishan, Eastern China Regional Background Station	27.58° N, 117.72° E, 1139 m a.s.l	2011.3–2012.2	2.70	1.48	0.55	(Su et al., 2013)
Dinghushan, South China Regional Background Station	23.2° N, 112.5° E, 100m a.s.l	2009.1–2010.12	13.6	6.5	0.48	(Chen, 2012)
Changbaishan, Northeast China Regional Background Station	42.4° N, 117.5° E, 736 m a.s.l	2009.1–2010.12	4.7	2.1	0.45	(Chen, 2012)
Fukang, Northwest China Regional Background Station	44.3° N, 87.9° E, 470 m a.s.l	2009.1–2010.12	8.3	2.2	0.27	(Chen, 2012)
Gonggar Mountain, Southwest China Regional Background Station	29.92° N, 102.61° E, 3541 m a.s.l	2017.1–2017.12	0.90	0.19	0.21	(Cheng et al., 2019)
Jinsha, Central China Regional Background Station	29.63° N, 114.2° E, 750 m a.s.l	2006.6–2007.7	5.6 ± 5.5	2.8 ± 5.5	0.5	(Lin et al., 2011)

\* indicates that the site is also one of the World Meteorological Organization (WMO) Global Atmosphere Watch (GAW/WMO) atmospheric background stations

**Table 3 Pearson correlations among NO<sub>x</sub>, SO<sub>2</sub>, and meteorological elements (daily average values).**

		NO <sub>x</sub>	SO <sub>2</sub>	WS	T	RH	P	MLD
NO <sub>x</sub>	annual	1	0.54*	-0.25*	-0.47*	-0.01	0.42*	-0.06*
	Spring		0.38*	-0.23*	-0.22*	0.09*	0.18*	-0.32*
	Summer		0.30*	-0.34*	-0.24*	0.04	0.25*	0.18*
	Autumn		0.46*	-0.28*	-0.36*	-0.06*	0.35*	-0.12*
	Winter		0.50*	-0.30*	0.06	0.09*	-0.07*	-0.22*
SO <sub>2</sub>	annual		1	-0.09*	-0.34*	-0.41*	0.39*	0.08*
	Spring			-0.05	-0.04	-0.41*	0.17*	-0.05
	Summer			0.00	0.07*	-0.32*	0.11*	-0.02
	Autumn			-0.11*	-0.23*	-0.56*	0.31*	0.12*
	Winter			-0.13*	-0.07	-0.34*	0.17*	0.02

Two-tailed significance test was used.

\*: Significant at 0.05 level of correlation

**Table 4 Annual percentage changes in NO<sub>x</sub> and SO<sub>2</sub> in various regions.**

<b>Location</b>	<b>Period</b>	<b>Base year</b>	<b>NO<sub>x</sub></b>	<b>SO<sub>2</sub></b>
LAN, this study	2006–2016	2006	–0.49 %/yr	–8.27 %/yr
YRD, China	2006–2016	2006	–0.45 %/yr	–6.65 %/yr
Pearl River Delta, China	2000–2019	2006	–2.84 %/yr	–3.93 %/yr
Wuhan City, China	2005–2017	2006	+2.08%/yr	–9.46 %/yr
North China	2005–2014	2005	–3.34 %/yr	–0.78 %/yr
Northwest China	2010–2016	2010	+12.98%/yr	–13.06 %/yr
New York city in America	2005–2016	2005	–3.46 %/yr	–5.97 %/yr
Kraków city in Poland	2005–2020	2007	–2.21 %/yr	–3.43 %/yr*
Preila station in Lithuania	2005–2017	2006	–1.60 %/yr	–6.83 %/yr
Louis Trichardt in South Africa	2005–2017	2006	+1.85%/yr	–5.11 %/yr
Amersfoort city in South Africa	2005–2017	2006	+6.50%/yr	+2.95%/yr